Submitted to: Dr. Y. S. Park
Office of Naval Research
Arlington, VA 2217

Final Report

"MeV Implantation Studies in LPE-grown GaAs and InP"

Contract No. N0001487K0799

Submitted by: C. R. Wie
Department of Electrical and Computer Engineering
State University of New York at Buffalo
201 Bonner Hall
Amherst, NY 14260

Period Covered: October 01, 1987 - March 31, 1989

ABSTRACT

Research has been conducted on growth and evaluation of high quality GaAs layer using Liquid Phase Epitaxy (LPE) and on MeV ion-implantation processings of Molecular Beam Epitaxy (MBE)-grown GaInAs layers on GaAs and LPE-grown GaAs layers on GaAs. By a novel growth method, i.e., isoelectronic doping of LPE GaAs layers with Indium, high structual and electrical quality layers were successfully grown. In the as-grown Indium-doped LPE GaAs layers, the etch pit density, rocking curve FWHM, and the ideality factor of a Schottky diode have improved significantly, showing an optimal In doping density of 2.4 x $10^{19}/cm^3$. The effects of MeV ion bombardment in a strained but partially relaxed GaInAs epitaxial layers on GaAs were systematically investigated. Depending on the state of initial relaxation, film thickness, and incident ion beam current, the lattice strain changed differently with the increasing ion beam dose. In a 1 MeV Si ion-implanted and 850 °C rapid thermal annealed GaAs layer on a n^+- or S.I.-GaAs substrate, we have measured the depth profiles of Hall mobility, carrier concentration, Schottky I-V-T behavior, and the deep level density. For the Au-Schottky diode made on the near-surface layer, conventional mechanisms dominated the current transport : recombination and diffusion currents under forward bias and generation current under reverse bias. Deep traps were not detected in the near-surface diode. For the Au-Schottky diodes made on the front and back shoulder of the damage peak in the depth profile curve, the current transport mechanisms changed to : tunneling current under reverse bias and an increased recombination current and the diffusion current under forward bias. Dominant traps were electron traps at E_c - 0.726 eV and 4 x

(1) → Gallium Arsenide, Indium Compounds.

10^{15} cm^{-3}. A room temperature 1 MeV oxygen ion-implantation at a dose of 1 x 10^{15} cm^{-2} produced a buried amorphous layers in InP near the end of range and a large number of recombination centers in the near-surface region of the GaInAsP epilayer as studied by a cross-section and high resolution electron microscopy and photoluminescene technique. X-ray rocking curve analysis showed a more uniform and less negative perpendicular mismatch in the surface of the GaInAsP layer.

I. Technical Summary

C. R. Wie
Department of Electrical and Computer Engineering,
State University of New York at Buffalo.

J. F. Chen, Research Assistant, Ph. D. completed in April 1989.

K. Xie, Research Assistant, Ph. D. expected in 1991.

1. LPE growth of In-doped GaAs and Characterization (reprint attached) :

With an objective of obtaining a high-quality starting material for the MeV ion-implatation study, we doped GaAs with Indium in a concentration ranging from 1×10^{19} to 1×10^{20} cm^{-3}. Liquid Phase Epitaxy techniques was used for the isoelectronic-doping and layer growth. For a 9 μm thick LPE GaAs doped with In, the surface morphology, rocking curve FWHM, and etch pit density improved with increasing In concentration in the range of 9×10^{18} to $2.4 \times 10^{19} cm^{-3}$. Above a 5×10^{19} cm^{-3} of In concentration, the structural quality of the epilayer and the eletrical property (leakage current of a Schottky diode) deteriorated. At the optimum indium concentration of 2.4×10^{19} cm^{-3}, a mirror-like surface morphology with no macroscopic terraces, about 0.003 deg FWHM for the rocking curve broadening, and a factor of 20 reduction in the etch pit density were achieved, which are a significant improvement over the undoped plain GaAs. At the optimum In concentration, the ideality factor in current-voltage characteristics of a Schottky diode was 1.04 over more than seven decades of current. The leakage current was also reduced substantially, and the overall I-V characteristics approached an ideal Schottky diode behavior

predicted by a thermionic emission and thermionic-field emission theory. The electrical behavior indicates a substantial reduction in background defect and electron trap densities.

2. MeV ion damage effect in the strained GaInAs epitaxial layer on GaAs (001) substrates (reprints attached) :

Various $Ga_{1-x}In_xAs/GaAs$ (001) single-layer samples were bombarded with 2 MeV He, 9 MeV P, or 15 MeV Cl ions and were characterized by the x-ray rocking curve technique and by the Raman technique. The composition was x = 0.07 - 0.15 and thickness was h ≈ 0.1 - 1.0 μm. For a thin layer (0.1 - 0.15 μm) which had an in-plane lattice mismatch of less than 0.01 % (i.e., nearly pseudomorphic), the ion bombardment, up to 10^{16} ions/cm^2 with the above ions, did not induce any further increase in the in-plane mismatch. However, the perpendicular mismatch decreased initially with beam dose at a low dose range and then increased at higher doses. The initial decrease of perpendicular mismatch was consistent with the increase in LO phonon frequency, both of which indicating a decreasing indium concentration in the GaInAs layer. At higher doses than a dose corresponding to 1 - 5 x 10^{17} KeV/cm^3 in damage energy deposition, the perpendicular mismatch increases and the phonon frequency decreases with increasing beam dose, which are expected in an ion-damaged III-V compound. At still higher doses, higher than a dose corresponding to 3 x 10^{19} KeV/cm^3 or 3 x 10^{20} KeV/cm^2 (depending on the ion beam current) in the damage energy deposition, the perpendicular mismatch drops precipitously by as much as 0.2 % in mismatch. However, there is no measurable change (i.e., less than 0.01%) in the in-plane mismatch. For the

well-relaxed GaInAs layers with a thickness of 1μm, there is no such precipitous strain decrease, and the lattice strain and phonon frequency behave very similarly to the bulk GaAs samples under ion bombardment.

3. Elecrical Characteristics of 1 - 1.5 MeV Si ion-implanted GaAs (reprint attached):

The electrical characteristics such as Hall mobility, carrier concentration, current transport mechanism, and deep electron traps, were measured after 850 °C RTA annealing. The depth dependence of these electrical properties were correlated with the ion-damage profile in the as-implanted samples.

Three diodes were made : one on the near-surface layer where the damage was predominantly point defects and complexes, one on the front shoulder of the damage peak, and one on the rear shoulder of the damage peak where the damage was the heavily disordered regions. The reverse I-V-T data clearly showed the current transport mechanism associated with the residual damage. The near-surface layer showed a predominant generation current, while the near-damage-peak layer showed a predominant tunneling current assisted by deep traps. The deep levels measured on the same diodes showed no measurable deep traps for the near-surface diode, and electron trap at E_c - 0.726 eV at 4 x 10^{15} cm^{-3} and hole trap at E_v + 0.806 eV at 1 x 10^{15} cm^{-3} for the near-damage-peak diodes. This work was performed to study the electrical effect of the residual defects after annealing. This clearly showed a need for further systematic research to establish the annealing condition for the optimum electrical performance of the ion-implanted GaAs.

The van der Pauw Hall measurement of the electron concentration and mobility in a 1.5 MeV Si implanted and 850 °C RTA annealed GaAs showed the following result. The electron concentration showed a depth-distribution which is expected from the range distribution of the Si dopents. However, the Hall mobility showed a broad minimum over the entire front shoulder of the carrier concentration peak. This again indicates a deteriated electrical performance of the material due to the not-yet-recovered extended defects in the heavily damaged region. This work produced the first data on the depth profiles of Hall mobility, current transport mechanism, and deep levels, in such MeV ion-implanted and annealed GaAs epitaxial layers.

4. 1 MeV Oxygen-implanted GaInAsP/InP (reprint attached) :

LPE-grown samples of $Ga_{0.18}In_{0.82}As_{0.38}P_{0.62}$/InP (001) were implanted with 1 MeV Oxygen ions at a dose of 10^{15} cm^{-2}. The as-implanted samples were characterized with Rutherford backscattering, photoluminescence, x-ray rocking curve, and high resolution and cross-section transmission electron microscopy. The 0.85 μm thick GaInAsP layer showed a strong luminescence peak at 1050 nm, corresponding to a bandgap of 1.181 eV. After bombardment, the peak completely disappeared, indicating that a large number of recombination centers were created. X-ray rocking curve showed a non-uniform lattice spacing in GaInAsP layer. After bombardment, the lattice spacing became more uniform. High resolution electron microscopy showed a buried amorphous layer near the end of ion range (~ 1.5 μm) within the substrate InP. The buried amorphous layer thickness was about 0.45 μm with crystalline InP on both sides.

II. Publications and Presentations

Publication

1. J.F. Chen, and C.R. Wie, "Structural and electrical contact properties of LPE grown GaAs doped with Indium", *J. Electr. Mater.* **17**, 501-508, (1988).
2. C.R. Wie, "Effects of MeV ion bombardment and thermal annealing on $Ga_{1-x}In_xAs/GaAs$", *Nucl. Instr. Meth.* **B37/38**, (1989), in press.
3. T.T. Bardin, J.G. Pronko, A.J. Mardinly, and C.R. Wie, "MeV ion implantation studies on LPE films grown on InP", *Nucl. Instr. Meth.* **B** , (1989), inpress.
4. C.R. Wie, G. Burns, F.H. Dacol, G.D. Pettit, and J.M. Woodall, "X-ray and Raman studies of MeV ion-bombarded GaInAs/GaAs", *Nucl. Instr. Meth.* **B** , submitted Feb. 1989.
5. K. Xie and C.R. Wie, "Structural and electrical characterization of MeV Si ion-implanted GaAs", *J.Appl.Phys.*, submitted April 1989.
6. C.R. Wie, K. Xie, G. Burns, G.D. Pettit, and J.M. Woodall, "X-ray and Raman studies of MeV ion-implanted GaInAs/GaAs", *Mater. Res. Soc. Symp. Proc.*, **Vol 104**, 499-504, (1987).
7. C.R. Wie, H.M. Kim, K. Xie, J.F. Chen, G. Burns, F.H. Dacol, G.D. Pettit, and J.M. Woodall, "Characterization of MeV ion-implanted GaInAs/GaAs using x-ray and Raman techniques", *SPIE proc.*, **VOL. 946**, 155-163, (1988).

Presentations

1. C.R. Wie, K. Xie, G. Burns, G.D. Pettit, and J.M. Woodall, "X-ray and Raman studies of MeV ion-implanted GaInAs/GaAs", presented at the MRS Fall Meeting, in symposium on Defects in Electronic Materials, Nov. 30 - Dec.3, 1987, Boston, MA.
2. C.R. Wie, H.M. Kim, K. Xie, J.F. Chen, G. Burns, F.H. Dacol, G.D. Pettit, and J.M. Woodall, "Characterization of MeV ion-implanted GaInAs/GaAs using x-ray and Raman techniques", presented at the SPIE conference on Spectroscopic Characterization Techniques for Semiconductor Technology III, March 14 -15, 1988, Newport Beach, CA.
3. C.R. Wie, "Effects of MeV ion bombardment and thermal annealing on $Ga_{1-x}In_xAs/GaAs$", presented at the 7th International Conference on ION IMPLANTATION TECHNOLOGY - IIT '88, June 7 - 10, 1988, Kyoto International Conference Hall, Kyoto, Japan.
4. T.T. Bardin, J.G. Pronko, A.J. Mardinly, and C.R. Wie, "MeV ion implantation studies on LPE films grown on InP", presented at the Tenth Conference on the Application of Accelerators in Research and Industry, Nov. 7 - 9, 1988.

Appedices

Reprints of Publications

Structural and Electrical Contact Properties of LPE Grown GaAs Doped with Indium.

Effects of MeV Ion Bombardment and thermal annealing on $Ga_{1-x}In_xAs/GaAs$.

MeV ion implantation studies on LPE films grown on InP.

X-ray and Raman studies of MeV ion-bombarded GaInAs/GaAs.

Structural and electrical characterization of MeV Si ion-implanted GaAs.

X-ray and Raman studies of MeV ion-implanted GaInAs/GaAs.

Characterization of MeV ion-implanted GaInAs/GaAs using x-ray and Raman techniques.

X-ray and Raman studies of MeV ion-bombarded GaInAs/GaAs

Chu R. Wie, State University of New York at Buffalo, Dept. of Electrical and Computer Engineering, Bonner Hall, Amherst, New York 14260

G. Burns, F.H. Dacol, G.D. Pettit, and J.M. Woodall,

IBM T.J. Watson Research Center, Yorktown Heights, New York 10598

ABSTRACT

We have measured elastic strains and longitudinal optical (LO) phonon shifts in MeV ion-bombarded single layers of (GaIn)As on GaAs(001). We have used He, P, and Cl ions, all in the MeV range, to bombard the samples and find that the elastic strains initially decrease with dose and the LO phonon frequency initially increases with dose. At higher doses, the strain increases and phonon frequency decreases, as expected for damaged GaAs crystals. For layers with negligible lattice relaxation (*i.e.*, with an in-plane mismatch less than 0.01%), a precipitous perpendicular strain release occurs at a high damage-energy deposition level. The in-plane mismatch for these samples, however, never changed over the same dose range. For 1 μm thick, well-relaxed layers, the beam-induced strain and phonon shift behave similarly to those in ion-damaged bulk GaAs crystals.

1. Introduction

Lattice mismatched strained heterojunction (GaIn)As/GaAs structures are drawing a considerable attention because of their applications in high speed devices [1-3], and there is fundamental interest with respect to the stability of such strained structures [4,5]. In processing such structures, ion implantation is an important step; however, it introduces damage and additional strains. Myers and coworkers [6] have carried out extensive characterization of keV ion-implanted strained-layer-superlattice (SLS) structures. MeV ions also have potential applications in processing devices with structures involving the strained layers. The MeV ion implantation introduces far less damage in the device-important surface layers than the low energy (keV range) ion implantions. Also, MeV energies drive the implanted dopants much deeper. The dominant defect species produced in the surface layers by MeV ion implantation are high density point defects and their clusters [7] as opposed to the disordered and amorphous regions which are produced by the keV ion implantations. Therefore, it is interesting to investigate the effects of MeV ion bombardment on strained epitaxial layer structures. We have studied the responses of strained epitaxial layers to the MeV ion-induced damages using the double crystal rocking curve (XRC, $CuK\alpha_1$ radiation) and Raman (wavelength=514.5 nm) techniques [10]. The results are presented in this paper.

2. Experimentals

$Ga_{1-x}In_xAs$ single layers were grown, by molecular beam epitaxy, on semi-insulating GaAs(001) substrates held at approximately 550 °C, on which a 0.5 μm thick GaAs buffer layer was first grown. The as-grown samples were

characterized by the XRC and Raman techniques before they were bombarded with various MeV ions. In Table 1, we list the sample (by number and by an alphabetical symbol for a plotting purpose) and then the x-value and thickness, h, are given. The last column lists the various ions and energies used in the subsequent bombardment. The indium content in the epilayer obtained by the XRC analysis, x(XRC), is listed in the fourth column and tends to be smaller than the nominal content, x, for most samples. There has been considerable discussion of the critical thickness of strained epitaxial films. The critical thickness, h_c, calculated under equilibrium conditions [8] is listed in Table 1 and in parenthesis we list the values calculated with an energy balance model [9]. Note the large difference between the values, and that our samples have thicknesses of the same order of magnitude as those calculated with the energy balance model. Those samples with a measured in-plane mismatch, ε_1^{xr}, of less than 0.01% are regarded as pseudomorphic in this paper, and these measured values are listed in the sixth column of Table 1.

The MeV ion irradiation was performed at room temperature with doses ranging from $5x10^{12}$ to $5x10^{15}$ ions/cm^2. The particle beam current was about 0.8-1 μA for 2 MeV He beam, 10 nA for 15 MeV Cl beam, and 2.5-10 μA for 9 MeV P beam. The rather high beam current for the 9 MeV P beam caused a significant beam-heating effect. The estimated beam-induced temperature rise was about 300 °C [10]. The estimated projected range [11] in GaAs is about 6.3 μm for 2 MeV He, 4.0 μm for 9 MeV P, and 5.3 μm for 15 MeV Cl beam. It is assumed that the MeV ion damage and induced strain are uniform in depth for the epitaxial layers with thicknesses up to 1 μm [15].

3. Results and discussion

X-ray rocking curves measure the lattice spacings of the epitaxial film

relative to the undamaged part of the substrate, in direction normal to the surface and in the two in-plane directions. From the lattice spacings, the elastic strains can be calculated under the assumption that a biaxial stress exists in the film [16]. We write the elastic strain (in the [001] direction perpendicular to the planar face) in an ion-damaged strained epitaxial layer as

$$\varepsilon_{zz}(x,D) = \varepsilon_{zz}(x,0) + \Delta\varepsilon_{zz}(D) \qquad (1)$$

where the first term on the right hand side is due to misfit in the as-grown undamaged layer and the second term is the beam-induced change. For the three psuedomorphic samples (*i.e.*, samples with the in-plane mismatch of less than 0.01%), in Fig.1 we plot the strain in the damaged strained epitaxial layer as a function of damage energy deposition (which equals the beam dose times the nuclear stopping power). Since, at the ion energies used in the present study, the nuclear stopping power is approximately constant over about 1 μm depth from the surface, we assume a uniform nuclear stopping power within the epitaxial layer and use its value at the surface, which can be found from the stopping power table [11] at the incident ion energy, in calculation of the damage energy deposition. At a low dose range, the elastic strain decreases with increasing beam dose until a damage-energy deposition of $5\text{x}10^{16} \sim 5\text{x}10^{17}$ keV/cm^3 is reached. Above this value of demage energy deposition, the elastic strain increases with increasing dose, as Figure 1 shows. The 9 MeV P and 15 MeV Cl ion-bombarded samples show a precipitous strain release at a damage energy deposition of around $3\text{x}10^{19}$ and $3\text{x}10^{20}$ keV/cm^3, respectively. The rough values of critical damage-energy deposition are indicated by vertical arrows in Fig.1. The maximum beam dose, $5\text{x}10^{15}$ ions/cm^2, for 2 MeV He ion (data symbol = "g") was not high enough to exceed this critical damage energy deposition. The factor 10 higher damage-energy deposition for the P ion beam than the Cl ion beam, to cause the precipitous strain release, is probably due to

the beam heating of the P beam induced by a high beam current. A precipitous stress release phenomenon was observed by Myers and coworkers [6] in an ion-implanted (GaIn)As/GaAs SLS samples. Their electron microscopy studies revealed that the stress release was accompanied by a formation of a dense dislocation network at the (GaIn)As - GaAs interface. However, from our measurements, the in-plane mismatch for the initially pseudomorphic samples did not increase beyond the XRC detectability limit (0.01%) at all beam doses.

We express, approximately, the total LO phonon frequency in an ion-damaged strained crystal as

$$\Omega(x,\varepsilon,D) = \omega_0(x) + \Delta\omega(\varepsilon) + \Delta\omega(D) \qquad (2)$$

where the first term in the right hand side is a bulk-equivalent frequency for undamaged crystal [12], second term is the Raman shift induced by the strain due to the lattice mismatch and ion-damage (see eq. (1)), and the third term is the beam-induced shift minus the beam-induced strain contribution. The strain-induced Raman shift is calculated from the measured elastic strain in the ion-bombarded sample by [13, 17]

$$\Delta\omega(\varepsilon) = [\, p\,\varepsilon_{zz} + q\,(\varepsilon_{xx} + \varepsilon_{yy})\,] / 2\omega_0 \qquad (3)$$

where p and q are the deformation constants and ε_{xx}, ε_{yy} and ε_{zz} are the elastic strains in [100], [010] and [001] directions, respectively. The LO frequency, $\omega_0(x)$, is obtained by subtracting the strain contribution from the Raman data in the as-grown samples [12]. This frequency is a function of the layer composition, and is listed in Table 1.

From the frequency Ω measured for the damaged crystal, we subtract the composition-dependent frequency $\omega_0(x)$ and the strain contribution $\Delta\omega(\varepsilon)$ so that we may have the frequency induced by lattice disorder only. In Fig.2, we plot

the damage-induced shift, $\Delta\omega(D)$, as a function of damage-energy deposition. The data symbols and the ion beams all correspond to the samples given in Table 1. The dashed horizontal line represents the phonon frequency of the undamaged as-grown samples. The data points above zero at lower doses, although they are above zero by a small amount, systematically indicate an increase of Raman frequency from the unbombarded-sample values. At higher doses, the frequency decreases as expected for the ion-damaged GaAs crystals [14]. The damage-energy deposition, at the transition from negative to positive frequency shift, is roughly $4x10^{18}$ keV/cm^3 for the 2 MeV He and 15 MeV Cl beam, and $4x10^{19}$ keV/cm^3 for the 9 MeV P beam (positions are indicated by arrows in the figure). The order of magnitude higher damage energy deposition level for the 9 MeV P beam is consistent with the higher damage-energy deposition level at the precipitous strain release seen in Fig.1, and already discussed. The large energy flux of the P ion beam, which probably increased the target temperature significantly, seems to cause a delayed damage-effect both in the precipitous strain release (see Fig.1) and in the Raman frequency decrease (see Fig.2).

In order to compare with the responses of the strained and unrelaxed samples, we bombarded some samples with well-relaxed epitaxial layers. In Figures 3 and 4, the damage-induced elastic strain and Raman shifts are shown as a function of 15 MeV Cl ion dose for 1 μm thick $Ga_{1-x}In_xAs$ layers with x=0.07 and 0.15 (samples 2 and 3 in Table 1). The initial lattice-relaxation in these films was such that the in-plane mismatch was $0.76\varepsilon_f$ for x=0.07 film and $0.86\varepsilon_f$ for the x=0.15 film, where ε_f is the misfit between the cubic unit cell (hence completely relaxed) for the layer and the cubic unit cell for the substrate. In these well-relaxed layers, the beam-induced elastic strain, $\Delta\varepsilon_{zz}(D)$,

which is shown in Fig.3 and the damage-induced phonon shifts, $\Delta\omega(D)$, which is shown in Fig.4, behave similarly to those observed in a bulk GaAs(001) crystal bombarded with 15 MeV Cl ions [7,14]. The bulk GaAs data are shown by a solid line in Fig. 3 for the elastic strain and by the data symbol "B" in Fig.4 for the Raman shift. In both figures, the horizontal line represents data for as-grown layers before bombardment. At low doses, a negative shift of elastic strain and a positive shift of Raman frequency are consistently observed.

4. Summary

We have presented data on the elastic strains and LO phonon shifts in MeV ion-damaged strained $Ga_{1-x}In_xAs$ layers of various thickness on GaAs. In layers with no observable in-plane mismatch (less than 0.01%), a precipitous strain release phenomenon is observed at a damage-energy deposition of about $3x10^{19}$ keV/cm^3. A negative Raman frequency shift is observed at a higher damage-energy deposition than about $4x10^{18}$ keV/cm^3. For a very high beam current (the 9 MeV P beam), the corresponding damage-energy deposition levels (for similar effects) were higher by roughly an order of magnitude. Well-relaxed layers show beam-induced shifts in strain and in Raman frequency which are similar to those observed in ion-damaged bulk GaAs crystals.

The SUNY-Buffalo portion of the work was supported by the Office of Naval Research under the contract number N00014-87-K-0799. C.R. Wie thanks his graduate students H.M. Kim and K. Xie for carrying out the rocking curve measurements.

References

1. J.J. Rosenberg, M. Benlamri, P.D. Kirchner, J.M. Woodall, and G.D. Pettit, IEEE Electron Dev. Lett. EDL-6, 491 (1985).
2. H. Ito and T. Ishibashi, Jap. J. Appl. Phys. 25, L421 (1986).
3. L.P. Ramberg, P.M. Enquist, Y.-K. Chen, F.E. Najjar, L.F. Eastman, E.A. Fitzgerald, and K.L Kavanagh, J. Appl. Phys. 61, 1234 (1987).
4. B.W. Dodson and J.Y. Tsao, Appl. Phys. Lett. 51, 1325 (1987).
5. P.L. Gourley, I.J. Fritz and L.R. Dawson, Appl. Phys. Lett. 52, 377 (1988).
6. D.R. Myers, G.W. Arnold, C.R. Hills, L.R. Dawson, and B.L. Doyle, Appl. Phys. Lett. 51, 820 (1987), and references therein.
7. C.R. Wie, T.A. Tombrello and T. Vreeland, Jr., Phys. Rev. B 33, 4083 (1986).
8. J.W. Matthews and A.E. Blakeslee, J. Cryst. Growth 27, 118 (1974).
9. R. People and J.C. Bean, Appl. Phys. Lett. 47, 322 (1985).
10. C.R. Wie, K. Xie, H.M. Kim, J.F. Chen, G. Burns, F.H. Dacol, G.D. Pettit, and J.M. Woodall, SPIE Proc. Vol. 946 (1988).
11. L.C. Northcliffe and R.F. Schilling, **Range and Stopping Power Table for Heavy Ions**, Nuclear Data Table 7, No. 3-4 (Academic Press, New York 1970).
12. G. Burns, C.R. Wie, F.H. Dacol, G.D. Pettit, and J.M. Woodall, Appl. Phys. Lett. 51 1919 (1987).
13. F. Cerdeira, C.J. Buchenauer, F.H. Pollak, and M. Cardona, Phys. Rev. B 5, 580 (1972).
14. G. Burns, F.H. Dacol, C.R. Wie, E. Burstein, and M. Cardona, Solid State Commun. 62, 449 (1987).
15. See, for example, Figure 1 and Figure 4 of reference 7.
16. Details for calculating the elastic strains from the x-ray rocking curve data are described in C.R. Wie, H.M. Kim, and K.M. Lau, SPIE Proc. Vol.877, p.41 (1988).
17. Parallel elastic strains can be obtained from $\varepsilon_{zz}/\varepsilon_{xx} = 2\nu/(1-\nu)$ where ν is the Poisson ratio.

Table 1 Characteristics of the as-grown $Ga_{1-x}In_xAs$ layers are given. Listed below are the sample numbers, nominal composition (x), nominal thickness (h), composition estimated from the x-ray data (x(XRC)), critical thickness (h_c), in-plane x-ray strain ($\epsilon_{\parallel}^{xr}$), misfit ($\epsilon_f$), perpendicular elastic strain (ϵ_{zz}), measured LO frequency (LO), bulk-equivalent LO frequency (ω_o), and the ion beam used.

Sample	x	h(nm)	x(XRC)	h_c(nm)	$\epsilon_{\parallel}^{xr}$(%)	ϵ_f(%)	ϵ_{zz}(%)	LO(cm^{-1})	ω_o(cm^{-1})	Ion beam
387(g)	0.10	150	0.095	15(298)	< 0.01	0.67	0.63	291.3	289.1	2 MeV He
389(h)	0.10	250	0.093	16(313)	0.32	0.66	0.32	290.0	288.9	2 MeV He
509(a)	0.12	110	0.102	14 (251)	< 0.01	0.74	0.67	292.2	289.8	9 MeV P
520(b)	0.12	140	0.089	17(346)	0.02	0.64	0.56	291.9	289.9	9 MeV P
519(c)	0.12	170	0.089	17(343)	0.03, 0.05	0.64	0.55	291.3	289.4	9 MeV P
508(d)	0.12	200	0.088	17(357)	0.07, 0.09	0.64	0.50	291.6	289.8	9 MeV P
510(e)	0.12	250	0.102	14(256)	0.21, 0.26	0.73	0.44	290.6	289.0	9 MeV P
1	0.07	100	0.084	18(396)	< 0.01	0.60	0.55	291.8	289.9	15 MeV Cl
2	0.07	1000	0.071	22(597)	0.39	0.51	0.10	289.9	289.6	15 MeV Cl
3	0.15	1000	0.107	13(224)	0.66	0.77	0.10	288.3	288.0	15 MeV Cl

FIGURE CAPTION

Fig. 1 The perpendicular elastic strain, ϵ_{zz}, of the damaged epitaxial layer is plotted for the three pseudomorphic films, as a function of the damage-energy deposition. The data symbols are listed in the first column of Table 1. The two vertical arrows indicate the rough positions of the precipitous perpendicular strain release.

Fig.2 The damage-induced LO phonon frequency shift is obtained by subtracting the bulk-equivalent frequency of an undamaged film and the strain-induced shift from the total measured frequency (see eq. 2). $\Delta\omega(D)$ is plotted here. The two vertical arrows indicate approximate positions of transition from positive to negative shift.

Fig.3 The beam-induced perpendicular elastic strain is obtained from the total measured perpendicular elastic strain[17] by subtracting the perpendicular elastic strain in an unbombarded as-grown sample. $\Delta\epsilon_{zz}(D)$ is plotted here (see eq. 1). Data are given for the two 1 μm thick, well-relaxed samples, "2" and "3" in Table 1. The solid curve is for a bulk GaAs(001) crystal bombarded with the same ion (taken from ref. 7). This figure shows that, under the ion bombardment, the 1 μm thick, well-relaxed layers behave similarly to the bulk GaAs(001) crystal.

Fig. 4 For the 1 μm thick, well-relaxed (GaIn)As films, the damage-induced LO phonon shift, $\Delta\omega(D)$, is plotted as a function of the bombarding ion beam dose. The data point "B" indicates the LO shift in a bulk GaAs(001) crystal under the same ion bombardment (taken from ref.11).

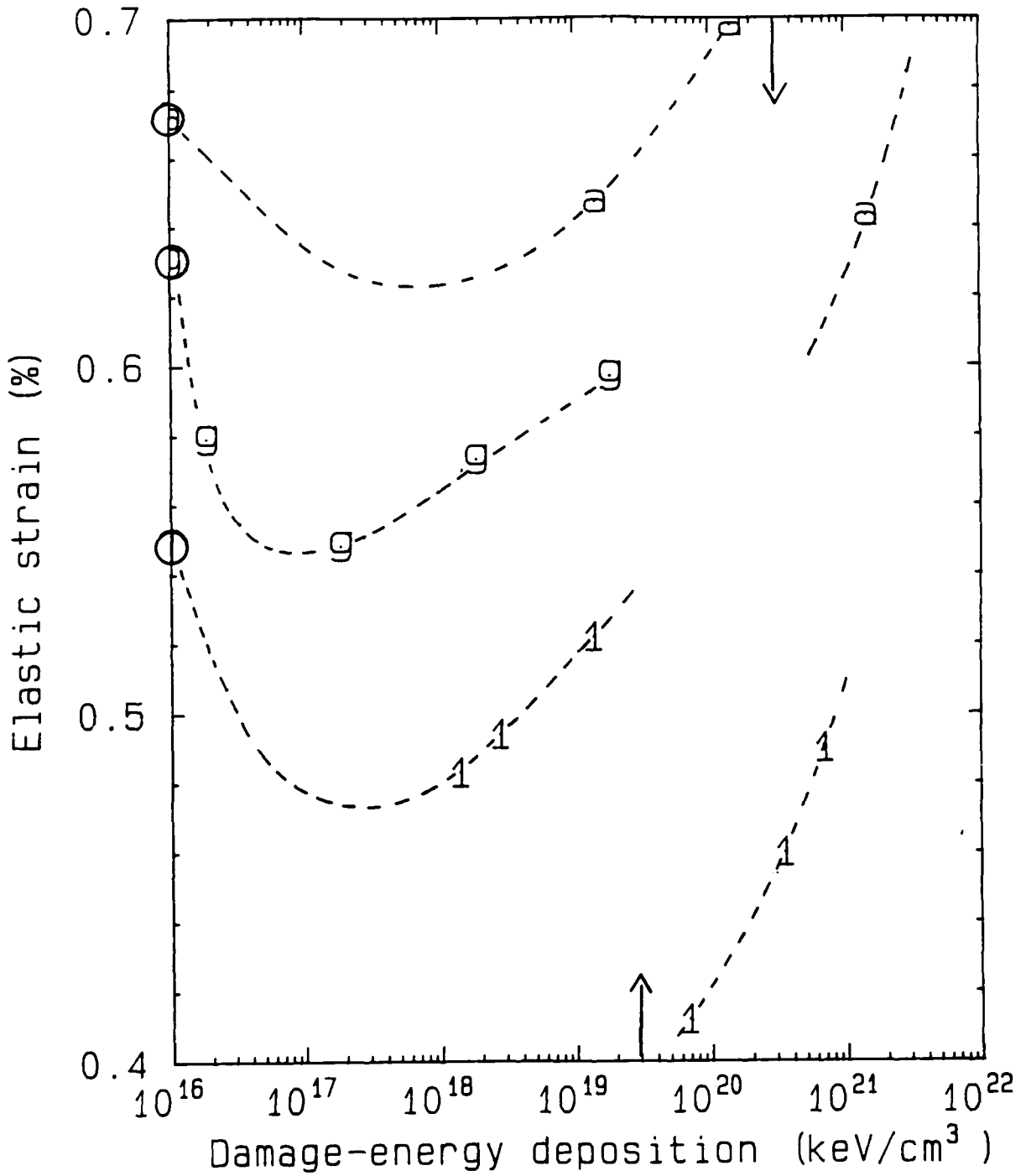
0.7
0.6
0.5
0.4
Elastic strain (%)
10^{16}
10^{17}
10^{18}
10^{19}
10^{20}
10^{21}
10^{22}
Damage-energy deposition (keV/cm^3)

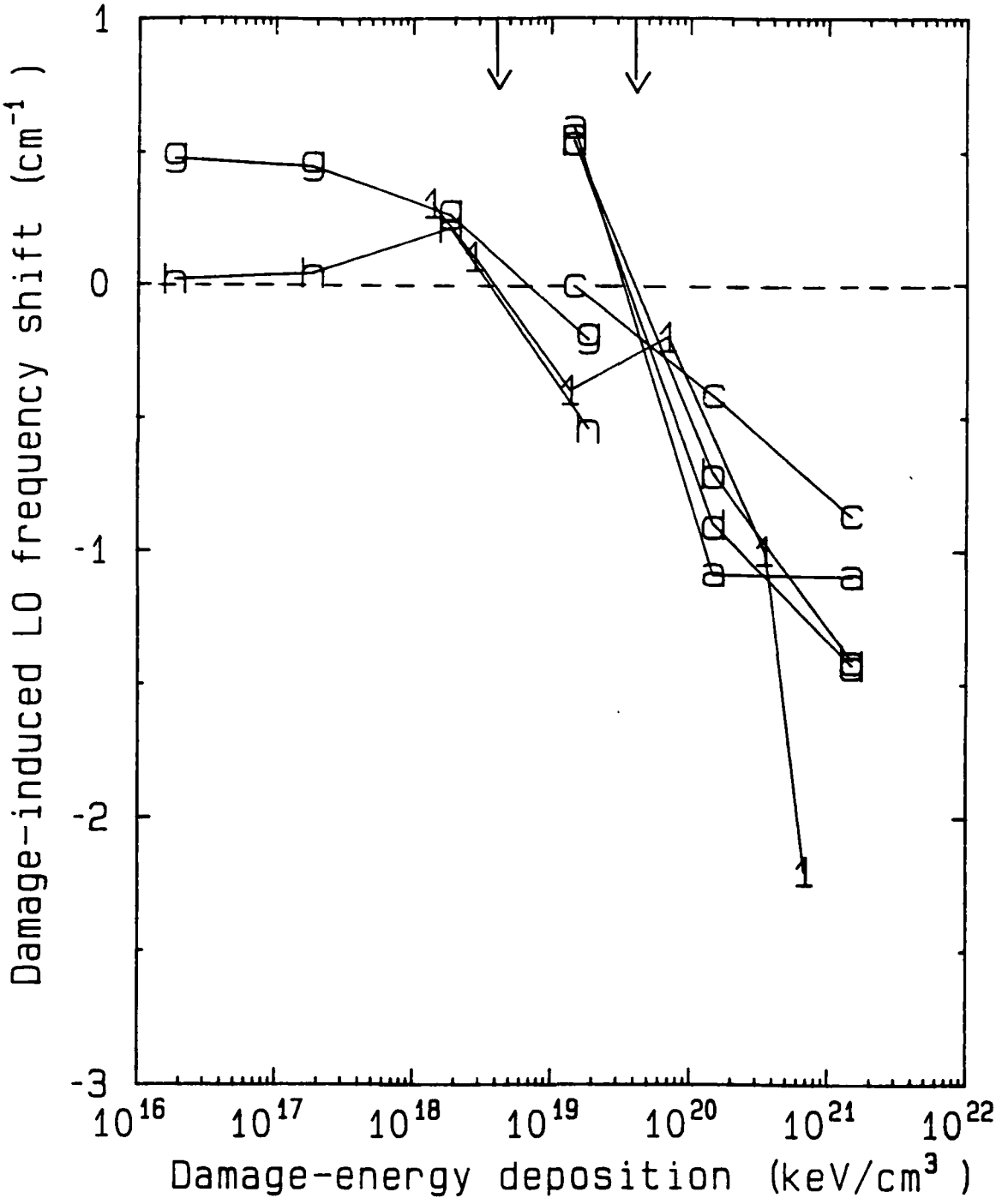
1
0
-1
-2
-3
Damage-induced LO frequency shift (cm^{-1})
10^{16}
10^{17}
10^{18}
10^{19}
10^{20}
10^{21}
10^{22}
Damage-energy deposition (keV/cm^3)

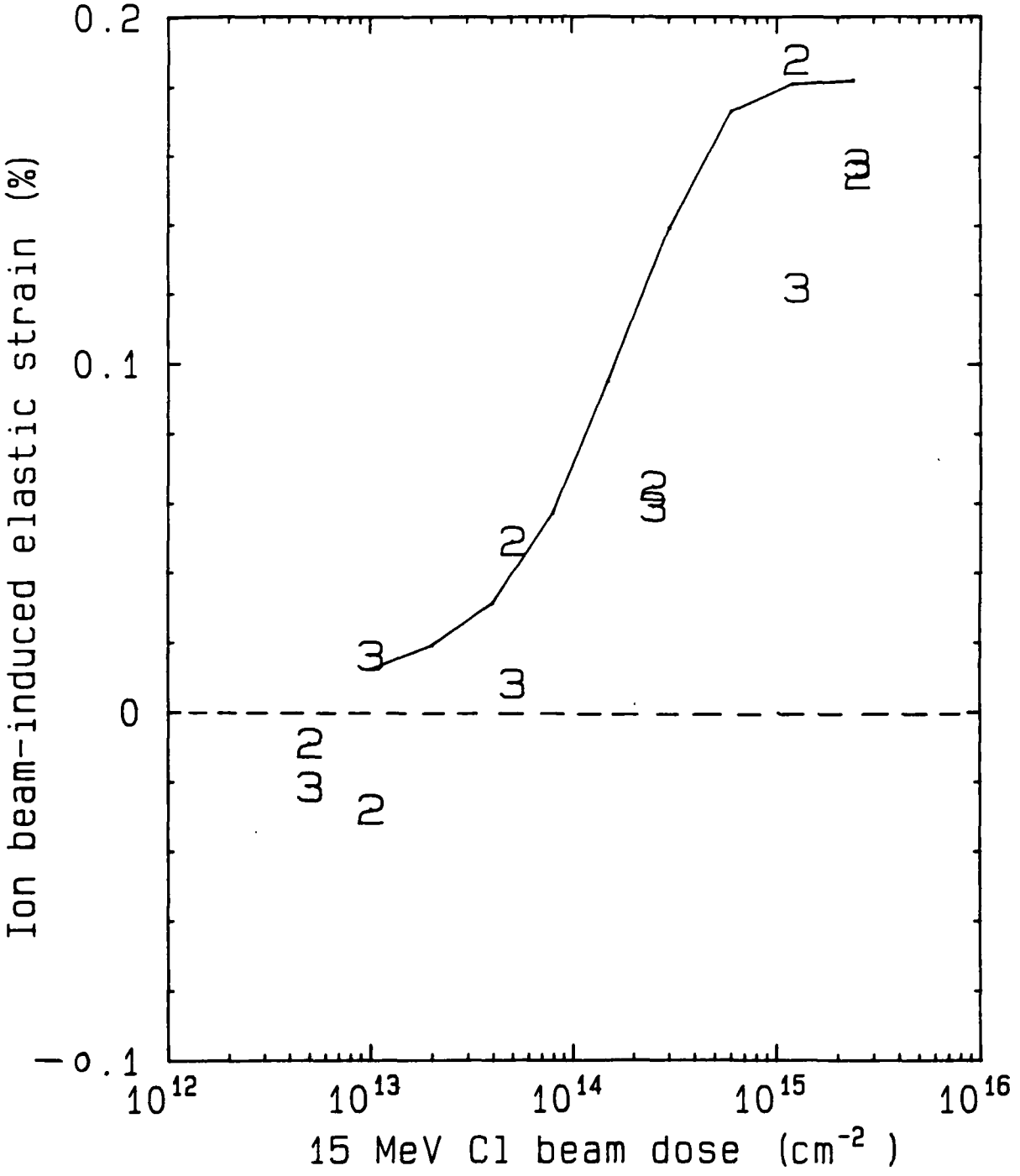
0.2
0.1
0
−0.1
Ion beam-induced elastic strain (%)
10^{12}
10^{13}
10^{14}
10^{15}
10^{16}
15 MeV Cl beam dose (cm^{-2})

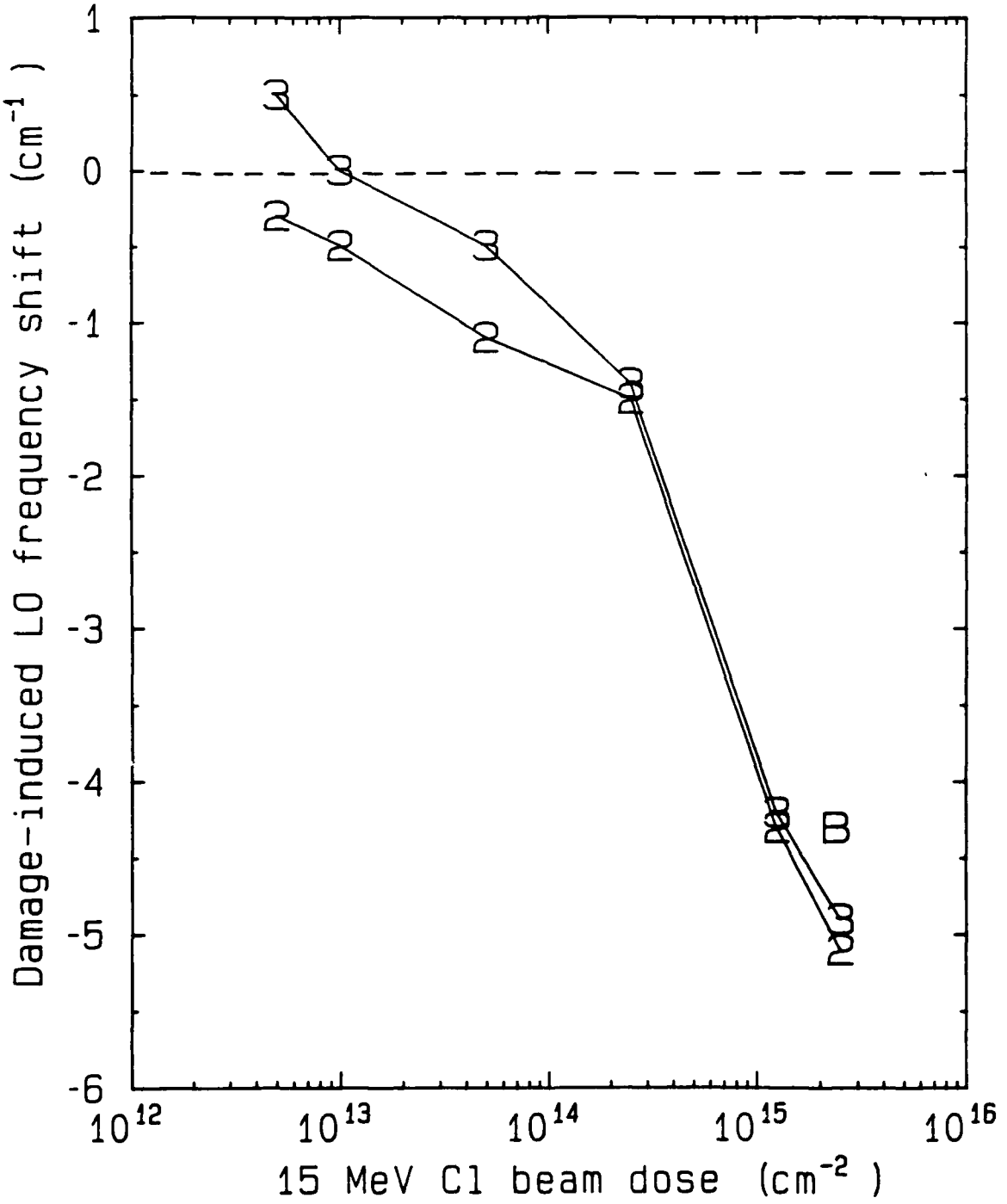
Damage-induced LO frequency shift (cm^{-1})
1
0
-1
-2
-3
-4
-5
-6
10^{12}
10^{13}
10^{14}
10^{15}
10^{16}
15 MeV Cl beam dose (cm^{-2})

MeV Si Ion-Implanted GaAs : Electrical Characteristics of Residual Damage

K.Xie and C.R.Wie
State University of New York at Buffalo,
Department of Electrical and Computer Engineering, Bonner Hall
Amherst, New York 14260

ABSTRACT

Structural and electrical characteristics of the MeV Si ion-implanted GaAs samples have been studied. The annealing behavior of strain and damage depth profiles is investigated using the x-ray rocking curve technique and the dynamical x-ray diffraction theory analysis. Photoreflectance spectra taken after rapid thermal annealing at 900^0c for 30s indicate the existence of many residual defects. The carrier concentration profile and mobility profile were obtained by van der Pauw Hall measurement and a successive chemical etching technique. Schottky diodes were formed at different depth along the ion path in the rapid thermal annealed sample. The I-V-T measurements show that different current transport processes dominate the reverse leakage current for diodes made at different depths. An electron trap was measured at E_C - 0.72 eV and 7E+15/cm^3 in the region of maximum damage.

I. INTRODUCTION

Ion implantation is an important technique in GaAs device fabrication. High energy (MeV) ion implantation has attracted much interest recently[1-3]. The fabrications of several GaAs device structures , such as slow wave device, mixer diode and voltage variable phase shifter, have been realized using direct MeV Si or S ion implantation[3-5]. Deep buried insulation layer and ion induced compositional mixing created by the MeV ion implantation have been successfully applied in the device fabrication[6]. The development of this technique requires better understanding of the problems, associated with high energy implantation, such as annealing process, damage recovery behavior, carrier profile, structure and distribution of resiual defects and correlation between residual defects and electrical properties. Some work on the annealing of damage and structure of defects in MeV ion-implanted III-V compounds has been reported[7,8,9]. It has been found that high density residual defects are mainly in the dislocation form. However, the effect of residual defects on the electrical properties has not been extensively studied. In this paper, we report the study of structural and electrical charateristics of MeV Si ion-implanted and annealed GaAs. For the 1.0 MeV or 1.5 MeV Si ion-implanted GaAs, the annealing behavior of a strain depth profile is presented. Correlation between residual defects and electrical properties has been made using differential Hall measurement, current-voltage measurement at various temperatures, and deep level transient spectroscopy (DLTS) measurement. The data demonstrate the effects of residual defects on mobility profile,

reverse leakage current, and deep levels.

II. EXPERIMENTAL PROCEDURES

Samples used in this study were the semi-insulating Cr-doped GaAS(100) wafers and liquid-phase-epitaxy (LPE) grown epitaxial GaAs layers on semi-insulating or n+ GaAs substrates. The n-type epilayers had carrier concentration of 5E+16/cm^3 or less, which was unintentionally doped, and a thickness of 3 um. The growth condition for different LPE samples was identical.

The semi-insulating wafers were implanted with Si ions at 1 MeV to various doses ranging from 1E+12/cm^2 to 3E+15/cm^2. Implantations in the LPE-grown epitaxial layers for the electrical study were performed at 1.0 MeV on a conducting substrate and at 1.5 MeV on a semi-insulating substrate. All implantations were carried out at room temperature and the samples were tilted to avoid channeling effects. The samples grown by LPE were annealed by rapid thermal annealing (RTA) at 900^0c for 30s with Si_3N_4 encapsulation. The samples exhibit no degradation of surface morphology after annealing.

X-ray rocking curves were taken from the as-implanted semi-insulating GaAs wafers using $FeKa_1$ radiation. Isochronal annealing was performed at a temperature ranging from 100^0c to 500^0c for 15 min at each 100^0c step under the forming gas flow. The rocking curves were taken after each annealing step. The strain and damage depth profiles were obtained by simulating rocking curves using the dynamical x-ray diffraction theory[10].

The carrier concentration profile and mobility profile were obtained from the van der Pauw Hall measurements after a successive chemical etching with a 5K Gauss magnetic field. The

sample for Hall mearsurements had a size of 0.7 * 0.7 cm^2, and the Omhic contacts were made by thermally evaporating Au-Ge and Ni through a metal mask and alloying in forming gas at 450^0c for 5 min. The sample was etched in a etchant of H_2O_2 : H_2SO_4 : H_2O in volume ratio of 2 : 2 : 100 with an etching rate of 700 $\pm$ 70 A/min. The contacts were protected by a photoresist during the chemical etching. The thickness of the layers removed was measured by a surface profiler.

In order to investigate the effect of residual defects on the current-voltage and deep level characteristics, the implanted epitaxial layer on an n+ substrate was etched to various depth. The surface of each step was located in the near surface region, or in the front shoulder (-0.75 μm from surface) or in the back shoulder (-1.15 μm from the surface) of the peak carrier concentration. Several Schottky diodes were made on each step with Au with an area of 0.785 mm^2. The current-voltage and DLTS measurements were conducted on all the diodes at each step to ensure the accuracy of results.

III.RESULTS AND DISCUSSIONS

Fig.1a shows the x-ray rocking curves for a symmetric (400) reflection from the 1 MeV Si ion-implanted GaAs (100). The peak located at zero angle is the substrate peak and the other peak(s) appearing at a negative angle are from the implanted region. From the analysis of experimental rocking curves using the dynamical x-ray diffraction theory, the strain depth profiles were obtained which are shown in Fig.1b. The maximum strain at the highest dose (3E+15/cm^2) is 0.43%, consistent with the saturation level

in ion-implanted GaAs[11]. The depth profile of total atomic displacment from the TRIM simulation, shown in Fig.2, shows a similar shape of curve and peak position. The Annealing behavior of strain depth profile for the sample implanted to a dose of 3E+15/cm^2 is shown in Fig.3, which was obtained from analysing each rocking curve taken after each annealing step. A total recovery of surface strain is found after annealing at 773 K. There is a small fraction of strain left in the region of maximum damage. X-ray rocking curves taken from the sample after rapid thermal annealing at 900^{0}c for 30s shows a complete recovery of strain. It is found that the recovery rate of strain is higher at a temperature around 500 K and around 700 K. It was noted by various authors that the vancancy recovery stage in GaAs is around 500 K[12] and the recovery stage of isolated antisite defects occurs over the range 700 K - 750 K[13]. It was also observed that a large, rapid reduction of defects in the near surface region takes place after annealing at 673 K[7]. The result of our measurement is in good agreement with those reports.

Photoreflectance measurement is sensitive to the crystal quality of the sample[14]. Fig.4 shows the photoreflectance spectra (PR) from an as-grown LPE sample and from the region close to the maximum damage in an 1.5 MeV Si ion-implanted sample which was annealed by RTA at 900^{0}c for 30 s. The signal from the as-grown sample shows a clear Franz-Keldysh (FK) oscillation. For the annealed sample, the PR signal is weak and FK oscillation smears out. This is attributed to the residual

damage in the implanted layer. X-ray rocking curve measurements of these samples show a higher value of full width at half maximum (FWHM) for the implanted, annealed sample than for the as-grown smple, indicating that the quality of implanted layer is still not totaly recovered after the anneal. Recently, there were a few transmission electron microscopy studies of MeV ion implanted GaAs[5,7,8]. The residual damage is found to exist in the region of maximum damage after annealing at 900^0c by the RTA technique. X-ray rocking curve and PR measurements on our samples all clearly indicate the existance of residual damage in the samples.

The depth distribution of carrier concentration and mobility are shown in Fig.5. The implanted ion profile calculated from the TRIM simulation is also shown in Fig.5. The peak position of carrier concentration profile compares well with the maximum peak position of calculated profile. There is a broadening in the back shoulder of the experimental profile. The channeling mechanism and thermal diffusion are likely to be the cause for this broadening. There is a decrease of mobility near the region where maximum nuclear stopping power is located. The mobility slightly increases in the tail region of the carrier concentration profile. The broad minimum in the mobility profile appears to be caused by the unannealed residual defect in that region. The sheet carrier concentration in that region was measured as a function of temperature. The result shows a small temperature dependence and seems to be affected by the presence of compensating centers. This phenomenon was reported on the insufficiently annealed samples[15,16].

Fig. 6 and 7 show the current-voltage characteristics of the Schottky diodes at different depth. One diode (diode 1) is at the near surface region, and two diodes (diodes 2 and 3) on the front and rear shoulders of the carrier concentration peak, respectively. In the forward bias case, diode 2 and 3 have a higher value of the ideality factor (n = 1.41 for diode 2 and n = 1.32 for diode 3) compared to the diode 1 which has the ideality factor close to 1 (n = 1.05) at the current range of 10^{-9} to 10^{-5} A. In the reverse bias case, diode 1 shows a low leakage current and little voltage dependence. Diodes 2 and 3 show a rapid increase of leakage current. It indicates that a strong field dependent mechanism dominate the leakage current transport of diodes 2 and 3. In order to understand the current transport mechanism, measurements were made for the temperature dependence of current-voltage characteristic. Fig. 8 is a plot of the reverse leakage current as a function of temperature for diode 1. There is a strong temperature dependence for diode 1 and little temperature dependence for diodes 2 and 3. The product of reverse current and capacitance for diode 1 is independent of reverse bias. It is clear that the generation current dominats the leakage current for diode 1. The generation-recombination center is at 0.42 eV below the conduction band edge as obtained from the slope of Fig.8. The voltage and temperature dependence of the reverse leakage current for diodes 2 and 3 indicate that neither thermionic emission nor generation is the principal mechanism[17]. Considering the presence of high concentration residual defects in these diodes, a trap-assisted tunneling model

seems to explain the leakage current of diode 2 and 3[18,19]. The model gives the following relationship between the current and applied reverse bias.

$$\ln(I_r) \propto A^*N_t^*V_b^{3/2} / (V_r+V_d)^{1/2}$$

where N_t is the total number of traps in the depletion region and V_b represents the energy barrier for the electron to tunnel through. A plot of $\log(I_r)$ versus $(V_r+V_d)^{-1/2}$ is shown in Fig.9 and clearly exhibits a linear dependence for both diodes. Therefore, the unannealed residual defects play a role in the current transport, by acting as a tunnel assisting center.

The DLTS measurements of these diodes were performed using Bio Rad DL4600. Various reverse biases were used during the measurements to ensure the accuracy of results[20]. Fig. 10 illustrates the DLTS spectra of the diodes 1, 2 and 3. There is no detectable electron traps in diode 1. The result of diode 1 was similar to our as-grown LPE samples with the same order of carrier concentration. The peak of the spectra of diode 2 and 3 coresponds to an electron trap with energy at Ec - 0.72 eV. The electron trap concentration in diode 2 is as high as 7E+15/cm^3 while it is more than an order of magnitude less in diode 3. We believe that this electron trap is caused by the residual defects in the heavily damaged region. Both current-voltage and DLTS measurements show the effcts of the residual defects in diodes 2 and 3 with the diode 2 exhibiting more effects.

IV.CONCLUSION

In summary, we have presented the structural and electrical

characteristics of 1.0 and 1.5 MeV Si ion-implanted GaAs. The annealing behavior of strain depth profiles were presented and they exhibit two annealing stages which are believed to be related to the recovery stage of vacancy at 500K and the recovery stage of antisite defects at 700K. Photoreflectance and rocking curve broadening reveal the existance of residual damage in the annealed samples. The carrier concentration profile from the differential Hall measurements was compared with the calculated range profile from the TRIM calculation and show a broadening of the rear-shoulder profile of the concentration peak in the experimental data. The residual defects seem to cause a broad minimum in the mobility profile. The residual defect is related to the high reverse leakage current of diodes through a trap-assisted tunneling mechanism. The DLTS measurements show a high concentration of electron traps in the large residual defect region. This is a clear indication of the role of residual defects in creating deep level. More systematic work are needed to minimize the effect of residual defects in the current transport, deep level and overall device performance. The search for the optimum annealing process to reduce the residual defect is an important future study.

ACKNOWLEDGMENTS

The authers are grateful to Harry B. Dietrich and P. E. Thompson of Naval Research Lab, and S.-Tong Lee and G. Braunstein of Eastman Kodak Co. for the Si implantation; G. Rajeswaran for

the rapid thermal annealing; J. Ziegler of IBM for the TRIM program; K. Jiao and W. A. Anderson for the DLTS measurement; Z. Shi and P. Hsieh for the Photoreflectance measurement; and J.F. Chen and Y. W. Choi for their assistances in the LPE growth and electrical measurments. This work was supported by the Office of Naval Research under the contract number N0001487K0799.

References

1. B.G. Streetman, IEEE Trans. on Nuclear Science NS-28, 1742 (1981).
2. Nathan W. Cheung, SPIE 530, 2 (1985).
3. Phillip E. Thompson, Harry B. Dietrich, and Michael Spencer, SPIE 530, 30 (1985).
4. C.M. Krowne and P.E. Thompson, Solid St. Electron. 30, 497 (1987)
5. Philip E. Thompson and Harry B. Dietrich, J. Electrochem. Soc. 34, 1240 (1988).
6. F. Xiong, T.A. Tombrello, T.R. Chen, H. Wang, Y.H. Zhang and A. Yariv, Appl. Phys. Lett. 54, 730 (1989)
7. S.-Tong Lee, G. Braunstein, and Samuel Chen, Mater. Res. Soc. Symp. Proc. 126, 183 (1988).
8. G. Braunstein, L.-R. Zheng, Samuel Chen, S.-Tong Lee, D.L. Peterson, K.-Y. Ko, and G. Rajeswaran, Mater. Res. Soc. Symp. Proc. (Dec. 1988).
9. S.J. Pearton, J.M. Poate, F. Sette, J.M. Gibson, D.C. Jackbson, and J.S. Williams, Nucl. Instr. and Meth. B19/20, 369 (1987).
10. C.R. Wie, T.A. Tombrello, and T. Vreeland, Jr. J. Appl. Phys. 59, 1743 (1986).
11. C.R.Wie, T. Vreeland, Jr. and T.A. Tombrello, Nucl.Instr. and Meth. B16, 44 (1986).
12. D.V. Lang, R.A. Logan, and L.C. Kimmerling, Phys. Rev. B15, 4874 (1977).
13. R. Worner, U. Kauffman, and J. Schneider, Appl. Phys. Lett. 40, 141 (1982).

14. N. Bottka, D.K. Gaskill, R.S. Sillmon, R. Henry, and R. Glosser, AIME 161 (1988).

15. J.M. Woodock, J.M. Shannon, and D.J. Clark, Solid State Electron. 18, 267 (1975).

16. N.G.E. Johansson and J.W. Mayer, Solid State Electron. 13, 317 (1970).

17. S.M. Sze, Phys. of Semiconductor Devices, 2nd ed. Wiley 1981

18. G.H. Parker and C.A. Mead, Phys. Rev. 184, 780 (1969).

19. J.M. Borrego and R.J. Gutmann, Appl. Phys. Lett. 28, 280 (1976).

20. Duncan Allsopp, Semiconductor Technology 2, 29 (1988).

Figure Captions

Fig.1.

a. X-ray rocking curves of 1 MeV Si ion-implanted GaAs(100). The peak at zero angle is the substrate peak. The peak(s) from the implanted region appear at the negative angle. b. The Strain depth profiles obtained from simulating the rocking curves using dynamical x-ray diffraction theory. The strain increase with the increase of ion dose.

Fig. 2.

The TRIM simulation of the depth profiles of total atomic displacments in GaAs implanted with 1 MeV Si. Compare this depth profile to the strain profiles in Fig.1

Fig. 3.

The depth profiles of strain after each annealing stap in 1 MeV Si ion-implanted GaAs (100). The dose is 3E+15/cm^2. The strain in the surface region recovers after a 773 K annealing.

Fig. 4.

Photoreflectance spectra at 300 K for an as-grown LPE sample and an 1.5 MeV Si ion-implanted LPE-grown sample annealed by RTA at 900^0c for 30s.

Fig. 5.

Profiles of the carrier concentration and mobility for 1.5 MeV Si ion-implanted GaAs grown by LPE. The dose is 5E+13/cm^2. The implanted ion profile calculated from TRIM simulation is also shown.It is noted that there is a broadening in the rear shoulder of carrier concentration profile.

Fig. 6.

Forward I-V characteristics for diodes 1, 2 and 3 on the sample of 1 MeV Si ion-implanted LPE-grown GaAs annealed by RTA at 900^0c for 30s. The diode 1 is at the near surface region and diodes 2 and 3 are located in the front and rear shoulders of the carrier concentration profile.

Fig. 7.

Reverse I-V characteristics for diodes 1, 2 and 3.

Fig. 8.

Temperature dependence of the reverse leakage current for the diode 1. The reverse current is at 1 V bias. The generation center is at -0.42 eV below conduction band edge as obtained from the slop of the plot.

Fig. 9.

Reverse current vs inverse of the electric field for diodes 1, 2 and 3. A linear relationship between the reverse current and the inverse of the electric field is observed.

Fig. 10.

DLTS spectra of the 1 MeV Si ion-implanted GaAs samples annealed by RTA at 900^0c for 30s. A electron trap is measured at E_c-0.72 eV. a. diode 2 with the trap concentration at 7E+15/cm^3, b. diode 3 with the trap concentration at 4E+14/cm^3 , c. diode 1 with no detectable traps.

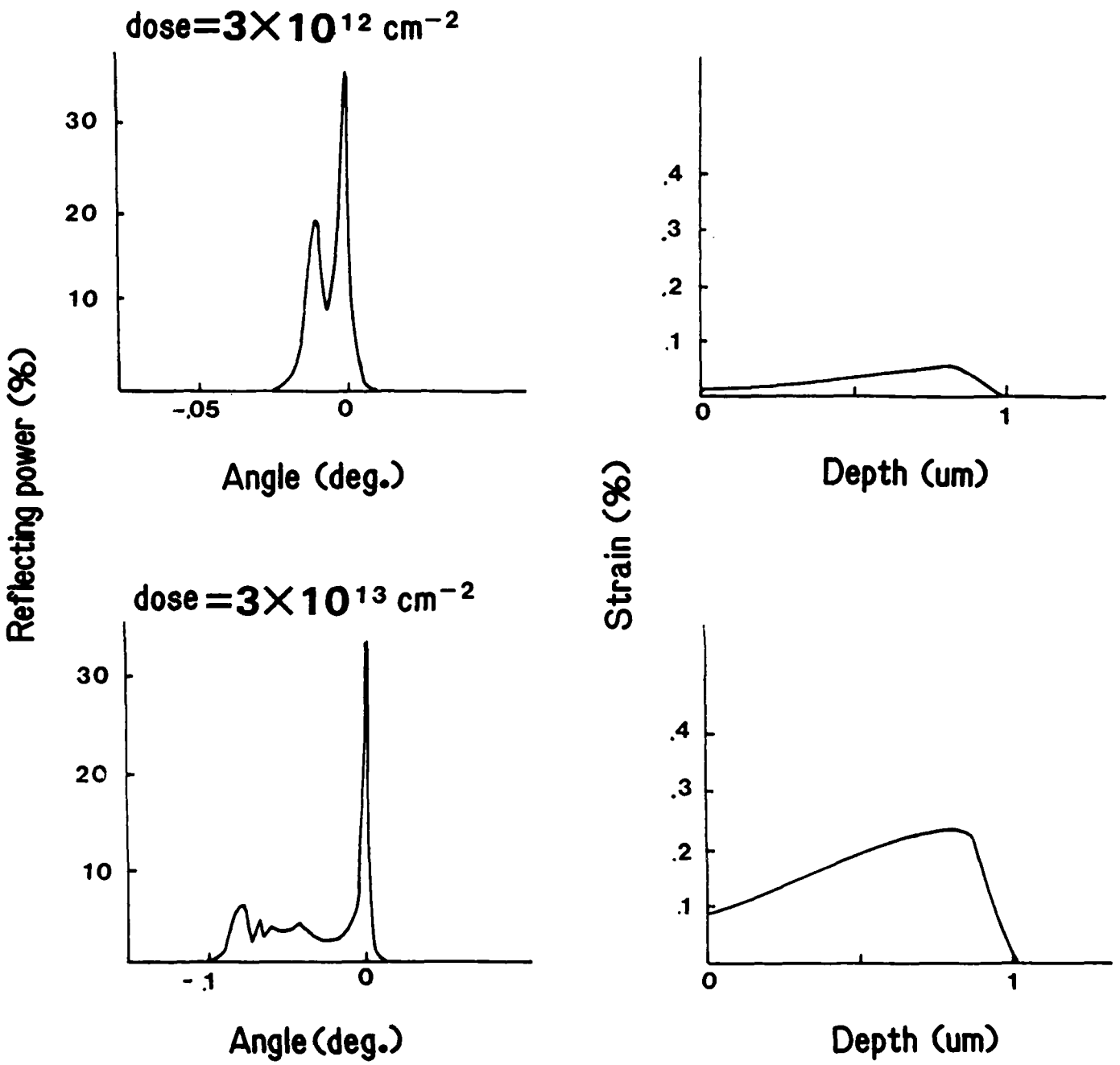
dose=3×10¹² cm⁻²
30
20
10
-.05
0
Angle (deg.)
Reflecting power (%)
.4
.3
.2
.1
0
1
Depth (um)
Strain (%)
dose=3×10¹³ cm⁻²
30
20
10
-.1
0
Angle (deg.)
.4
.3
.2
.1
0
1
Depth (um)
(a)
(b)

Fig. 1

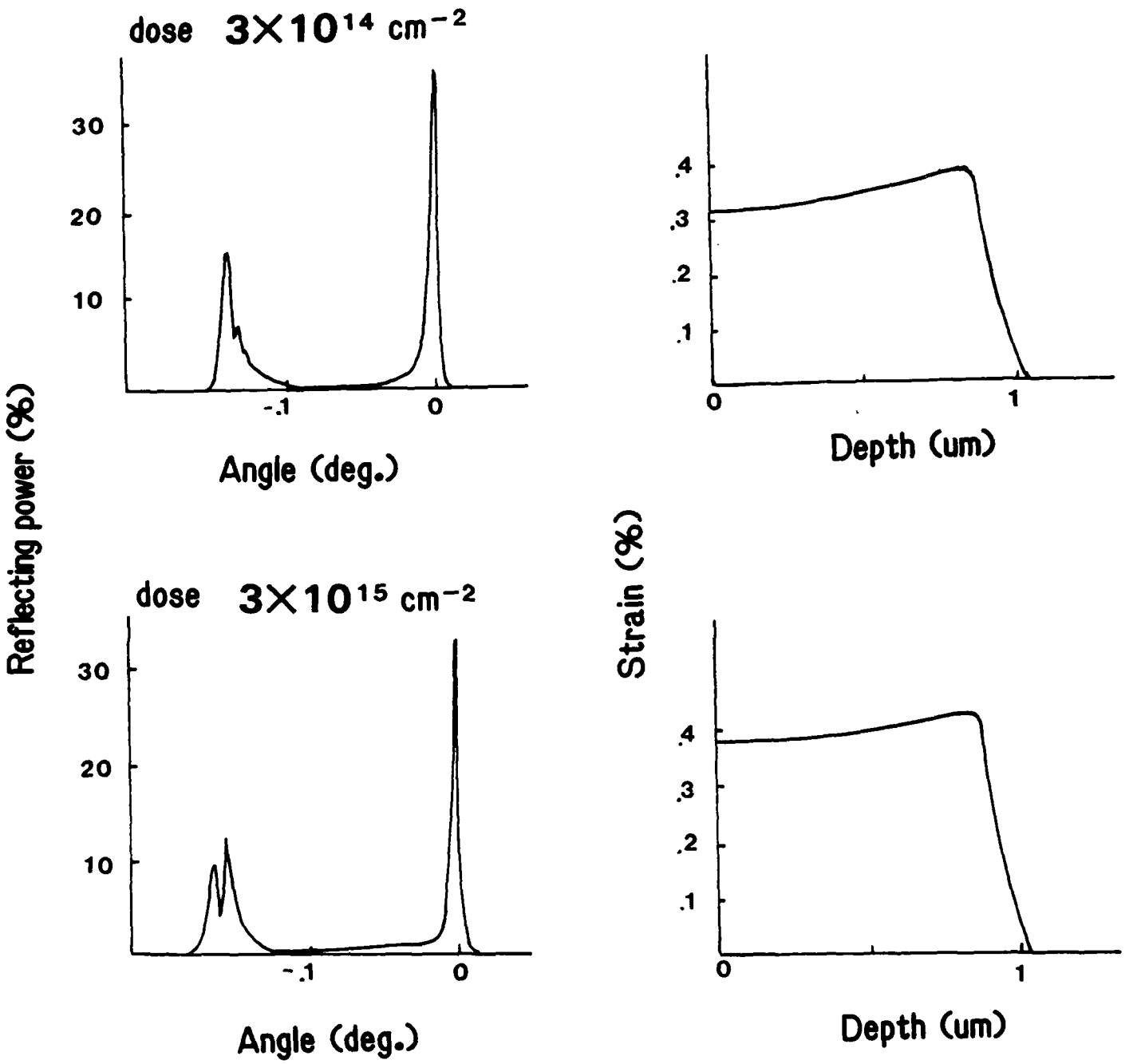
dose 3X10^14 cm^-2
30
20
10
-.1
0
Angle (deg.)
.4
.3
.2
.1
0
1
Depth (um)
Reflecting power (%)
dose 3X10^15 cm^-2
30
20
10
-.1
0
Angle (deg.)
Strain (%)
.4
.3
.2
.1
0
1
Depth (um)
(a)
(b)

Fig. 1

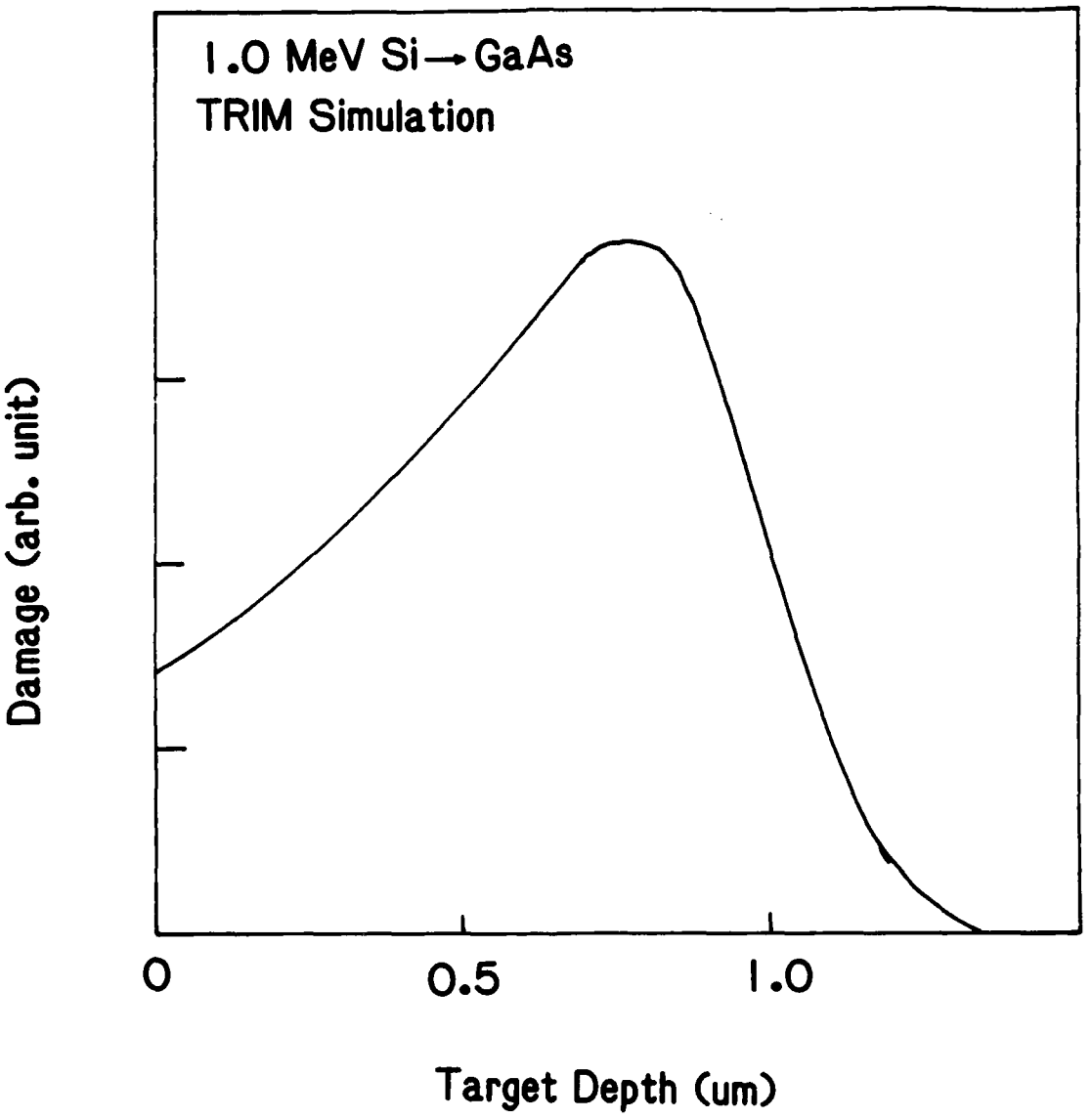
1.0 MeV Si → GaAs
TRIM Simulation
Damage (arb. unit)
0
0.5
1.0
Target Depth (um)

Fig.2

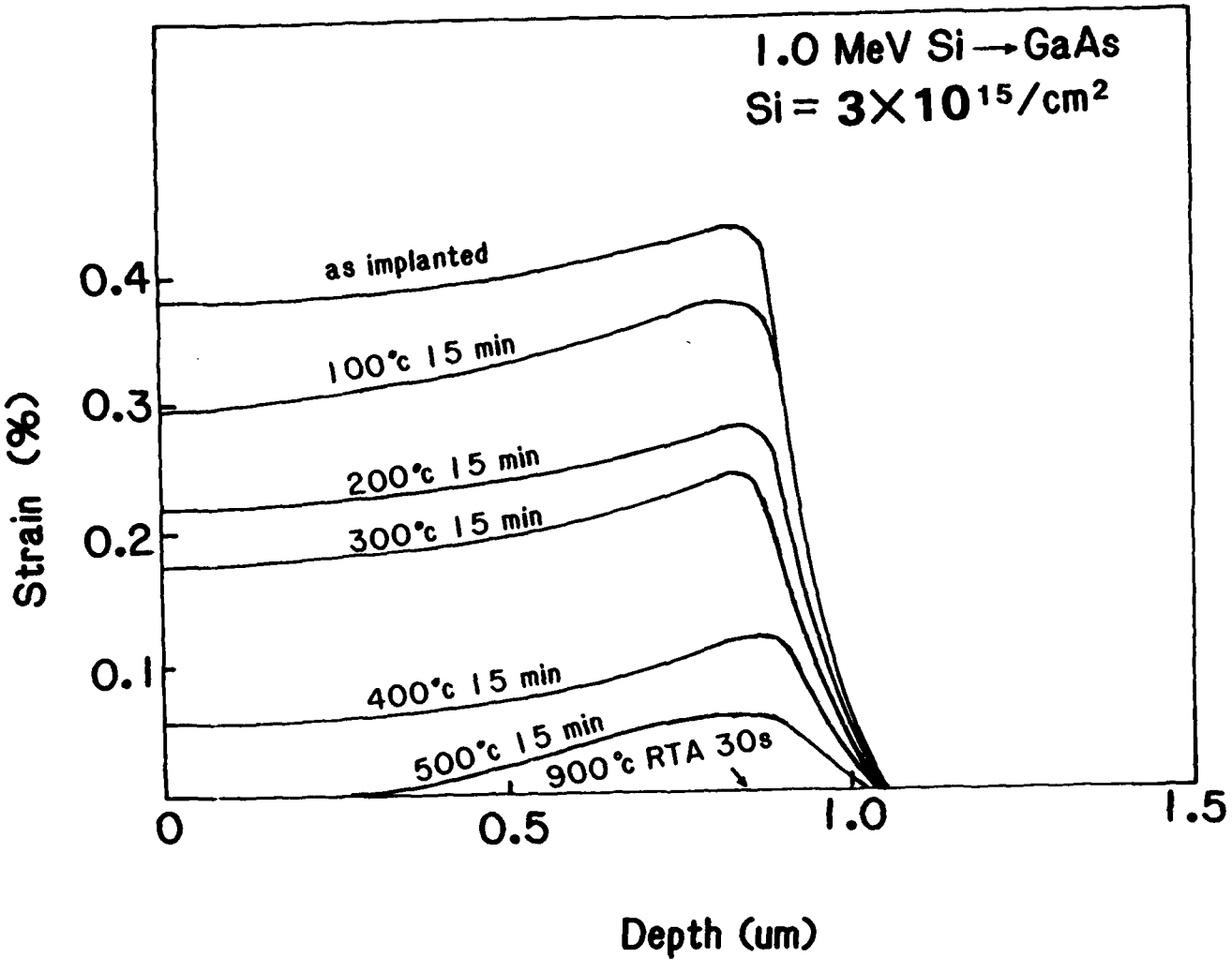
1.0 MeV Si → GaAs
Si = 3×10¹⁵/cm²
as implanted
100°c 15 min
200°c 15 min
300°c 15 min
400°c 15 min
500°c 15 min
900°c RTA 30s
Strain (%)
0.4
0.3
0.2
0.1
0
0.5
1.0
1.5
Depth (um)

Fig.3

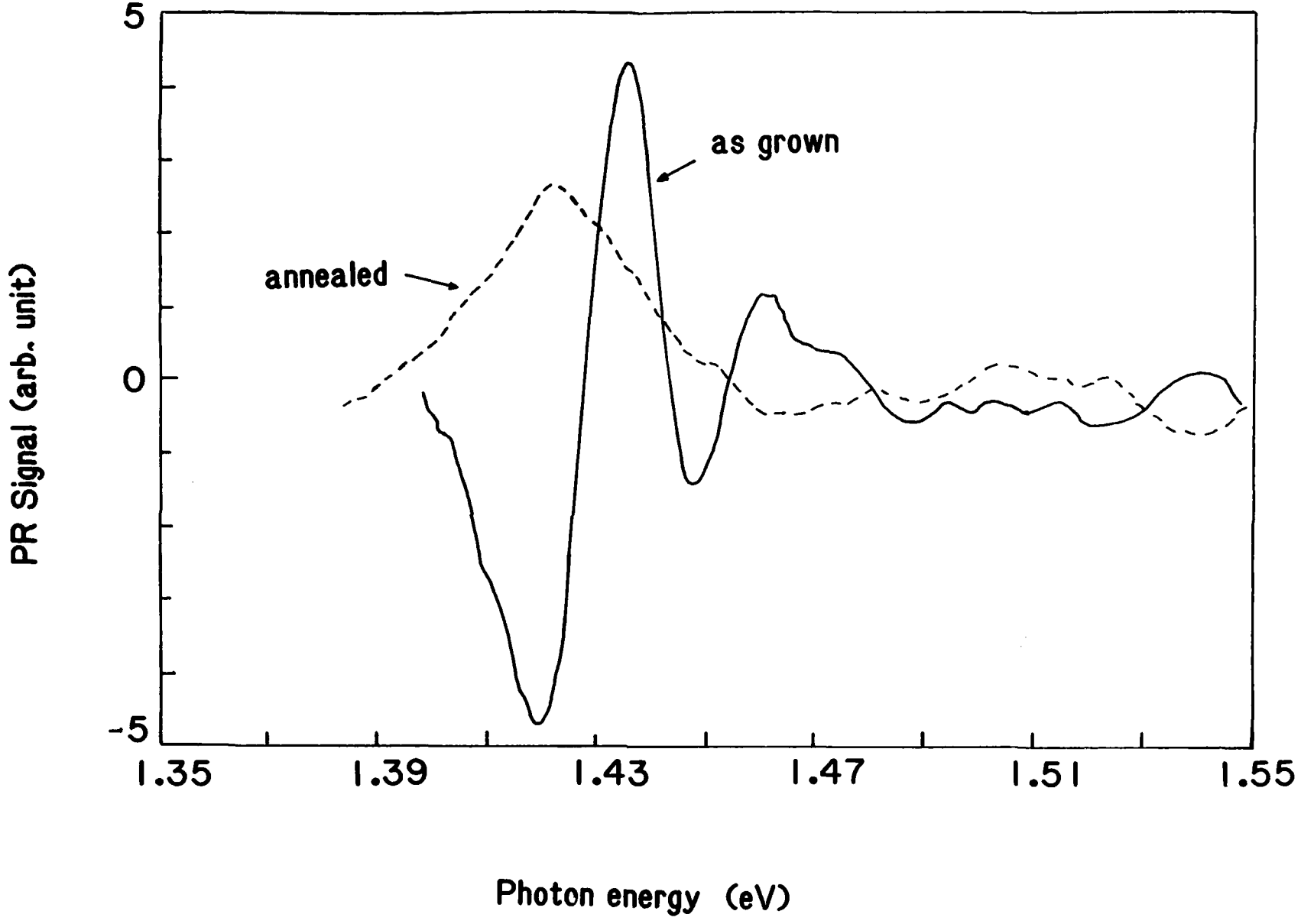
5
0
-5
PR Signal (arb. unit)
as grown
annealed
1.35
1.39
1.43
1.47
1.51
1.55
Photon energy (eV)

Fig.4

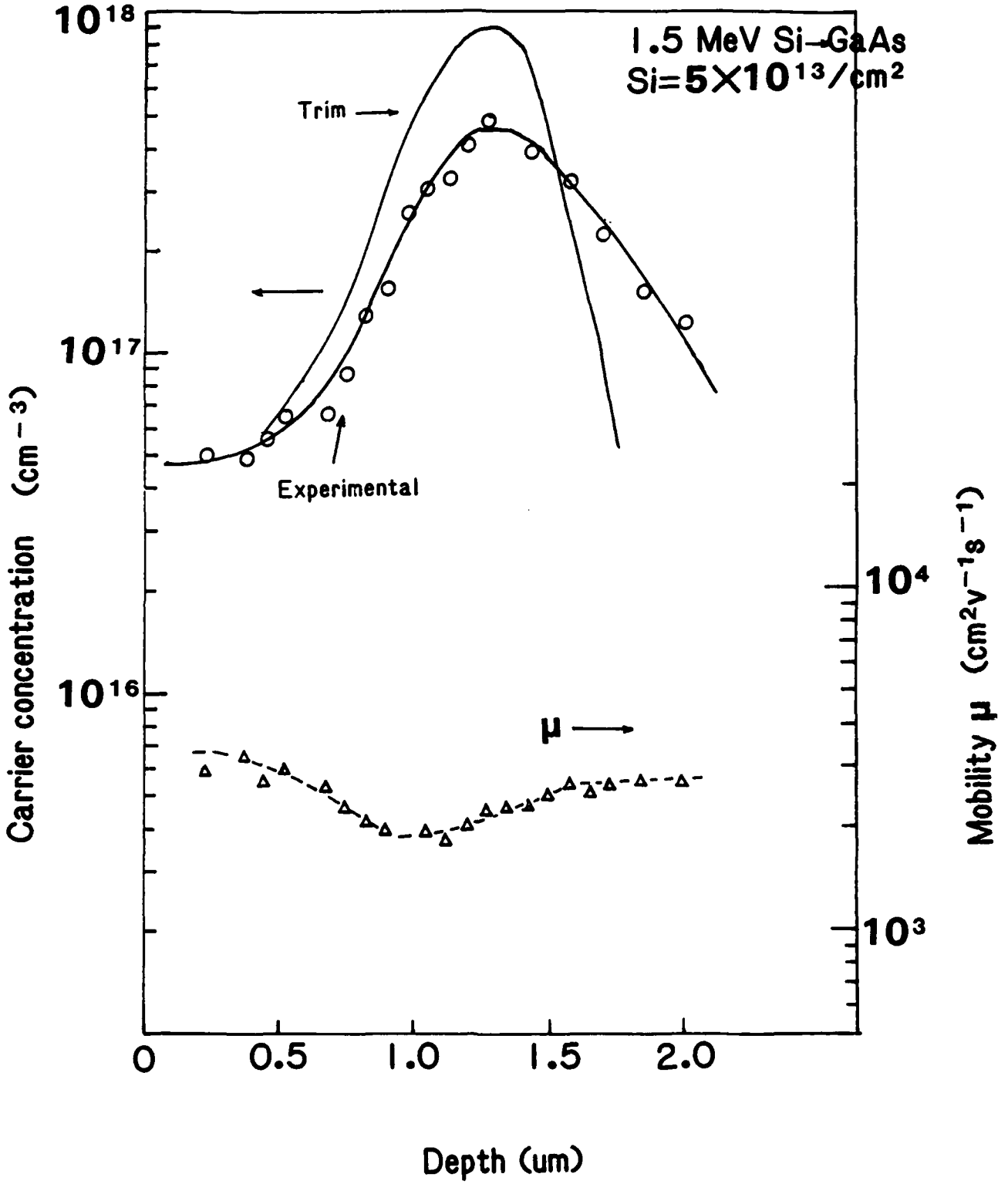
1.5 MeV Si→GaAs
Si=5×10¹³/cm²
Trim
Experimental
μ
10¹⁸
10¹⁷
10¹⁶
10⁴
10³
0
0.5
1.0
1.5
2.0
Carrier concentration (cm⁻³)
Mobility μ (cm²v⁻¹s⁻¹)
Depth (um)

Fig.5

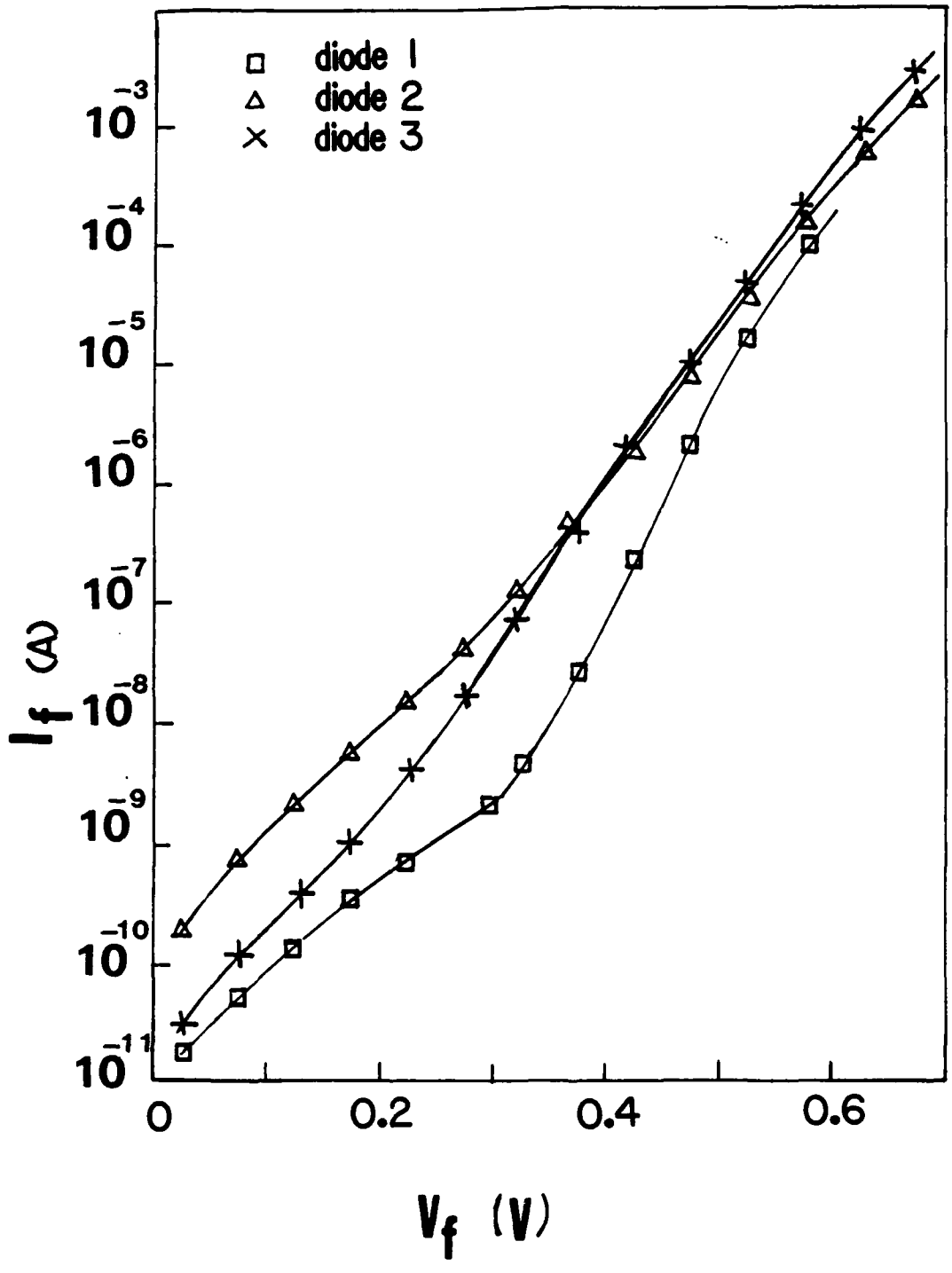
diode 1
diode 2
diode 3
10^{-3}
10^{-4}
10^{-5}
10^{-6}
10^{-7}
10^{-8}
10^{-9}
10^{-10}
10^{-11}
I_f (A)
0
0.2
0.4
0.6
V_f (V)

Fig.6

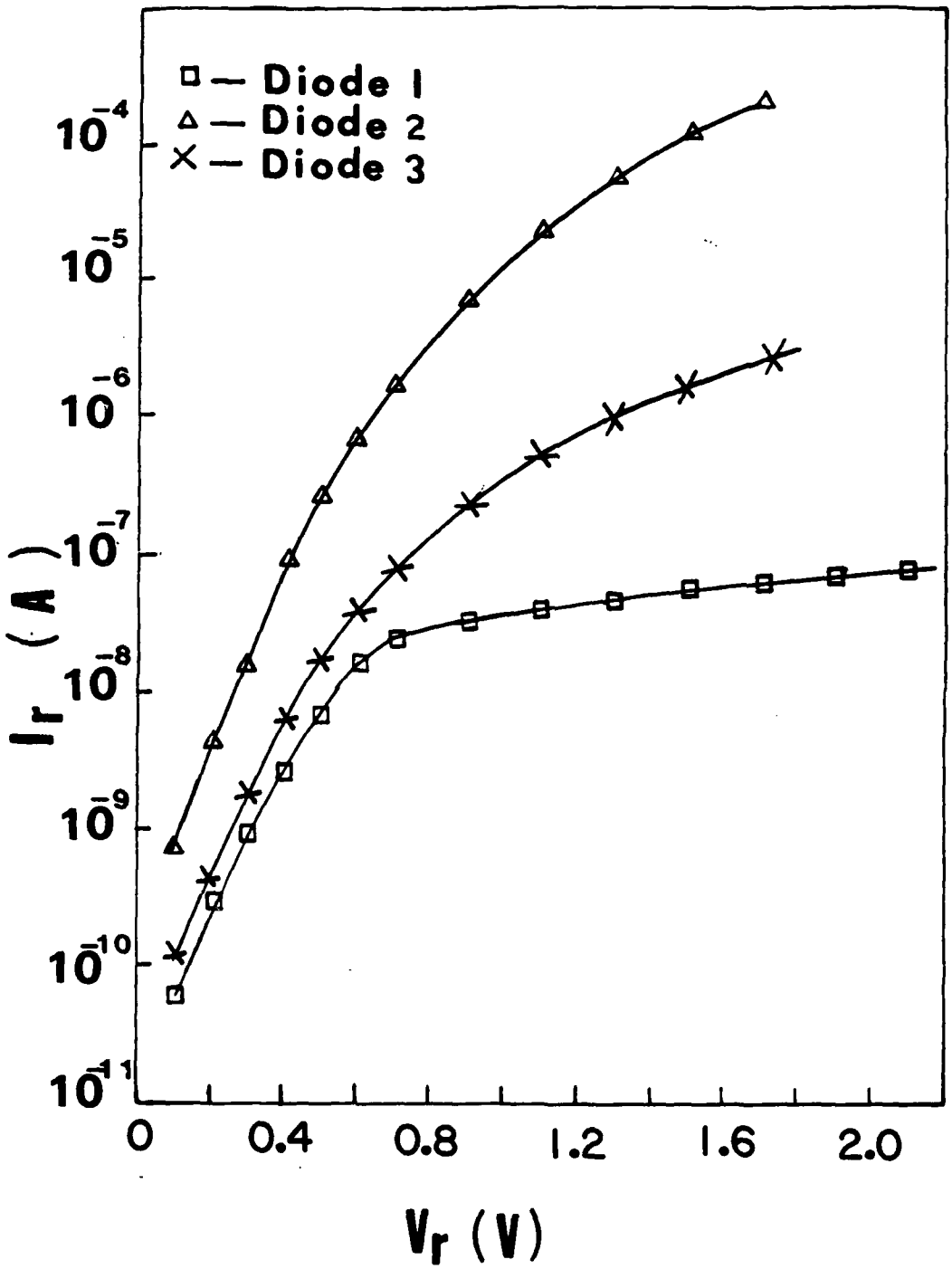
□ — Diode 1
△ — Diode 2
× — Diode 3
10^{-4}
10^{-5}
10^{-6}
10^{-7}
10^{-8}
10^{-9}
10^{-10}
10^{-11}
I_r (A)
0
0.4
0.8
1.2
1.6
2.0
V_r (V)

Fig.7

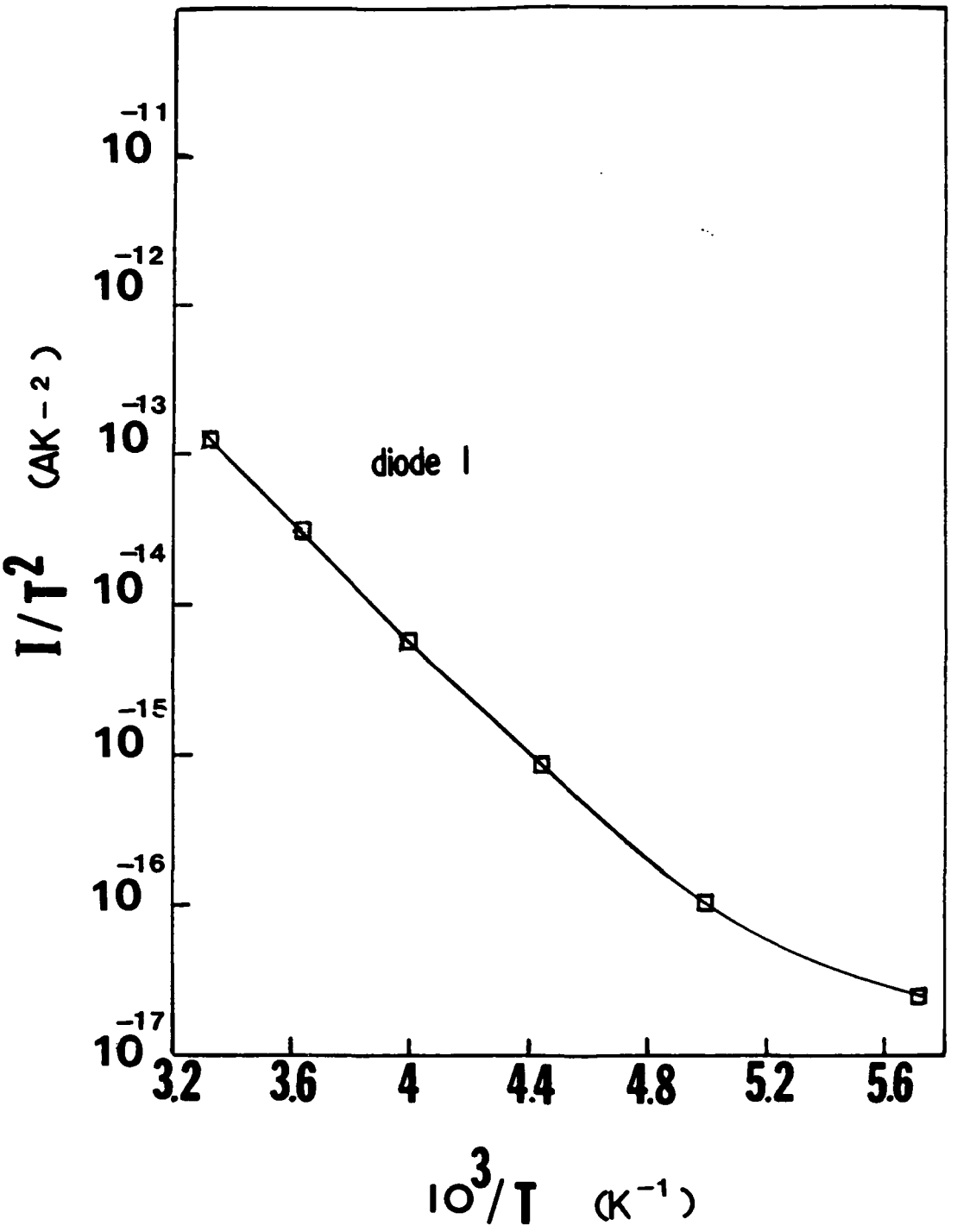
10^{-11}
10^{-12}
10^{-13}
10^{-14}
10^{-15}
10^{-16}
10^{-17}
I/T^2 (AK^{-2})
diode I
3.2
3.6
4
4.4
4.8
5.2
5.6
$10^3/T$ (K^{-1})

Fig.8

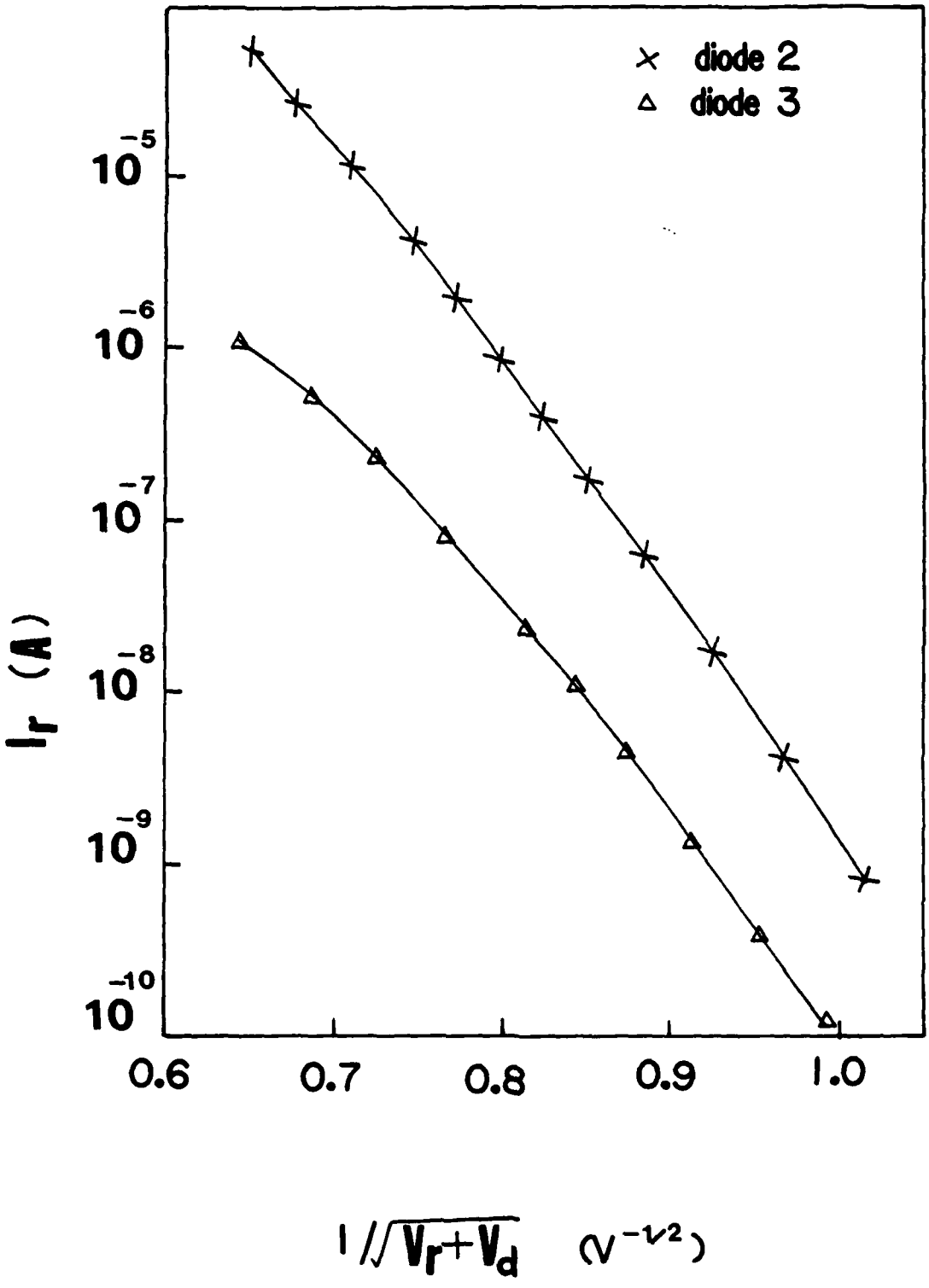
diode 2
diode 3
10^{-5}
10^{-6}
10^{-7}
10^{-8}
10^{-9}
10^{-10}
I_r (A)
0.6
0.7
0.8
0.9
1.0
$1/\sqrt{V_r+V_d}$ $(V^{-1/2})$

Fig.9

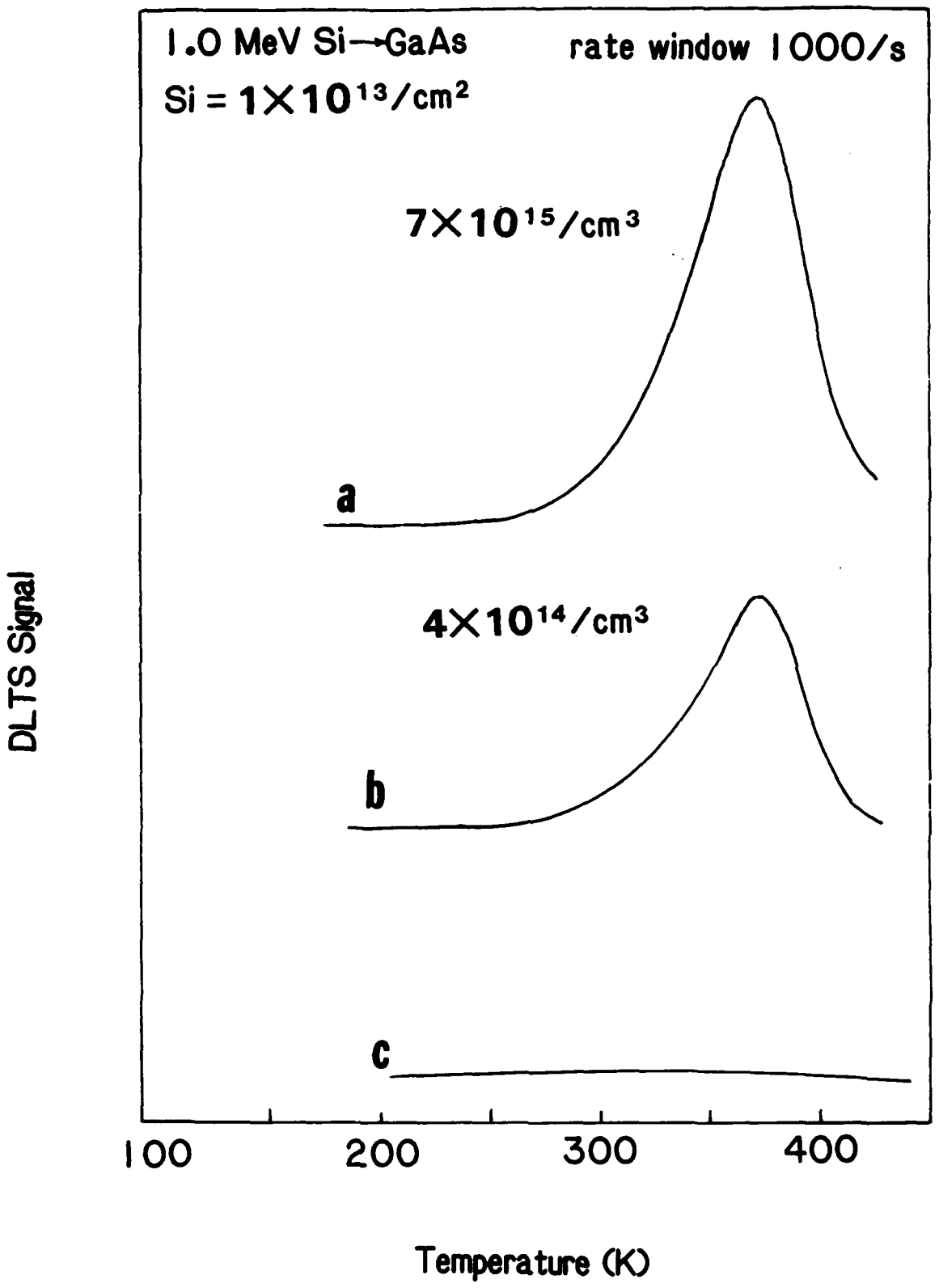
1.0 MeV Si→GaAs
rate window 1000/s
Si = 1×10¹³/cm²
7×10¹⁵/cm³
a
4×10¹⁴/cm³
b
c
DLTS Signal
100
200
300
400
Temperature (K)

Fig. 10

Effects of MeV ion bombardment and thermal annealing on $Ga_{1-x}In_xAs/GaAs$*

Chu R. Wie, State University of New York at Buffalo, Dept. of Electrical and Computer Engineering, 201 Bonner Hall, Amherst, New York 14260

ABSTRACT

We have measured the lattice constants of the deformed unit cells of $Ga_{1-x}In_xAs$ single layers on GaAs(001) substrates after bombardment with various MeV ions and/or after thermal annealing. The x-ray rocking curve data indicate a substantial loss of indium from the (GaIn)As layer as a result of MeV ion bombardment or thermal annealing. This observation demonstartes the necessity of a proper protective cap layer against the indium out-diffusion during the treatments. For the (GaIn)As layers with an initial in-plane mismatch of less than 0.01%, a high level damage-energy deposition from the MeV ion bombardment leads to a precipitous decrease of the perpendicular lattice constant, where as there is no change in the in-plane lattice constant. For these films, the in-plane mismatch does not change under the MeV ion bombardment or a thermal annealing up to 500°C. We also report the behavior of in-plane mismatch for various relaxed-layers under ion bombardment or thermal annealing.

* This work was supported in part by the Office of Naval Research under the contract number N00014-87-K-0799.

1. Introduction

MeV ions are drawing an increasing attention as an extension of the ion implantation technology [1]. Important parameters in the implantation technology are the range distribution of the implanted dopants and the distribution, characteristics and anneal behavior of the implantation-induced damage [2]. For MeV ions, these parameters are yet to be studied for a more reliable processing technology. Also, since the epitaxially grown homojunction or heterojunction layers are essential components of most III-V semiconductor devices, it is interesting to study the damage characteristics produced in these epitaxial layers by the MeV ion implantation [3].

2. Experimental

The $Ga_{1-x}In_xAs$ layers used in this study were grown by molecular beam epitaxy on GaAs(001) substrates held at 550 °C. We list, in Table 1, the sample number, x-value, layer thickness (h), in-plane mismatch (or parallel x-ray strain) of the as-grown samples, and the ion beams used for the bombardments. One sample ("g" in Table 1) was used only for heat treatment. Throughout this paper, we use the sample number as the data symbol in the figures. The beam currents and the mean ion depths are 0.8 - 1.0 μA and 6.3 μm for 2 MeV He, 2.5 - 10 μA and 4.0 μm for 9 MeV P, and about 10 nA and 5.3 μm for 15 MeV Cl beam. The relatively high beam current of the P beam, induced a significant sample heating during the ion bombardment (corresponding to about 300 °C). After bombardment, the samples were analyzed by the x-ray rocking curve technique which measured the parallel and perpendicular lattice constants of a (GaIn)As film relative to a GaAs(001) substrate. The lattice constant measurements provide information on the lattice mismatch at the interface and on the composition change in the epi-layer caused by the treatment. Elastic

strains can be obtained using the x-ray strains, and they are reported in ref.4 for the samples studied here. For some samples, the Raman technique was used to measure the beam-induced shift of LO phonon frequency, and we present the Raman data for a comparative study with the rocking curve data. Thermal annealing was performed on some as-grown layers and some ion-bombarded samples, and these samples were analyzed using the same techniques.

3. Effects of MeV ion bombardment

3.1 The in-plane mismatch

The relative lattice constant difference in the plane of interface is the parallel x-ray strain (or in-plane mismatch), which is presented in Fig.1 for the layers with an initial mismatch greater than 0.01 %. The x-ray rocking curve technique is capable of measuring the in-plane mismatch, reproduceably, if it is greater than 0.01%. Films with an in-plane mismatch less than 0.01 % are treated as pseudomorphic films in this paper. For the pseudomorphic films ("1", "a", and "g" in Table 1), the in-plane mismatch did not increase after the ion bombardment, staying constant at 0% ± 0.01%.

For films with an in-plane mismatch greater than 0.01%, we show, in Fig. 1, the behavior of the in-plane mismatch as a function of the bombarding beam dose. The data points in an open circle are the pre-bombardment values. For the 2 MeV He bombarded sample, "h", the in-plane mismatch varied by about 0.06% over the dose range. For the 9 MeV P bombarded sample which had an initial in-plane mismatch of 0.02%, "b", the in-plane mismatch varied by less

than 0.02% over the dose range. For layers, "c" and "d", with an initial in-plane mismatch of o.o4% and 0.08%, respectively, the in-plane mismatch varied somewhat randomly between 0.01% and 0.07% over the dose range $5x10^{13}$ - $5x10^{15}$ cm^{-2} of the 9 MeV P beam. A layer with an initial mismatch of 0.24%, "e", relaxed substantially further upon the P ion bombardment to an in-plane mismatch of 0.44% ± 0.03% after the ion bombardment. This was a sample which showed a clear beam-induced relaxation phenomenon. The two 1 μm thick layers, "2" and "3", bombarded with 15 MeV Cl ions showed a significant variation in mismatch over the beam dose range $5x10^{12}$ - $2.5x10^{15}$ cm^{-2}. The one with a lower x-value (x=0.07) decreased and the one with a higher x-value (x=0.15%) increased in the in-plane mismatch with the beam dose.

We could find no systematic trend in the in-plane mismatch with the MeV ion bombardments. However, the in-plane mismatch, for the (GaIn)As films with initial values less than 0.01%, did not increase after the ion bombardments with the He, P, or Cl beam.

3.2 The perpendicular lattice constant

In Fig. 2 and Fig.3(a), we show the behavior of the perpendicular x-ray strain with an ion bombardment. In Fig.2, we plot the perpendicular x-ray strain as a function of the damage-energy deposition. The three samples shown here are the pseudomorphic films, "1", "a", and "g" in Table 1. It is seen, in Fig.2, that the perpendicular lattice constant of a pseudomorphic (GaIn)As film initially decreases with the ion bombardment, reaching a minimum at a damage-energy deposition of 10^{17} - 10^{18} keV/cm^3. Since the parallel x-ray strain for these films did not increase, remaining within 0.01%, the decrease in

the perpendicular lattice constant relates to a decrease in the unit cell volume, which, in turn, implies loss of indium from the (GaIn)As layer. A Raman measurement showed a small increase in the LO phonon frequency [4] over a similar range of damage-energy deposition over which the perpendicular x-ray strain decreases, which, according to the LO phonon frequency versus composition curve in ref. 5, implies a decrease in the indium content of the (GaIn)As layer.

At higher levels of damage-energy deposition, the perpendicular lattice constant increases with the MeV ion bombardment, due to an increasing damage level. The indium loss may still occur; however, the radiation damage dominates the lattice constant change in this high level of damage-energy deposition. At an even higher beam dose, the perpendicular lattice constant decreases precipitously at a damage-energy deposition of ~ $3x10^{19}$ keV/cm^3 for the 15 MeV Cl beam and ~ $3x10^{20}$ keV/cm^3 for the 9 MeV P beam. The slower response to the radiation damage of the P ion-bombarded sample is ascribed to a beam-induced heating effect (~ 300 °C). A precipitous stress release phenomenon was also observed by Myers and coworkers in an ion-implanted (GaIn)As/GaAs strained layer superlattice [6]. Their electron microscopy study revealed a formation of dense network of interface dislocations accompanying the precipitous stress release. However, our observations show no increase in the parallel lattice constant of the (GaIn)As film at the precipitous strain release.

In Fig.3, we show the perpendicular x-ray strain and the LO phonon frequency shift from an unbombarded value for the 1 μm thick, well-relaxed layers, "2" and "3". The solid curve in Fig.3(A) is the perpendicular x-ray strain

data (taken from ref. 7), and the datum point "B" in Fig.3(B) is the phonon frequency shift for a bulk GaAs(001) crystal bombarded by the same ions (taken from ref. 8). Both figures indicate that the 1 μm thick films behave similarly to a bulk GaAs(001) crystal under the MeV ion bombardment. The rather highly scattered data points for the perpendicular x-ray strain, shown in Fig. 3(A), gave much less scattered data for the elastic strain which was obtained by considering the parallel x-ray strain as well (see ref. 4). The elastic strain seemed to be a better parameter to characterize the ion-damaged strained epitaxial layer.

4. Effects of thermal annealing

4.1 Annealing of unbombarded as-grown (GaIn)As

An unbombarded 1 μm thick (GaIn)As layer, the sample "i" in Table 1, was isochronally annealed for 15 minutes at 300 °C and at 500 °C. The in-plane mismatch after both annealing steps was found to be fixed at 0.45 % ± 0.01 %, independent of temperature. However, the depth-averaged perpendicular x-ray strain was 0.743 % at room temperature, 0.726 % after the 300 °C annealing, and 0.722 % after the 500 °C annealing. This shows a small decrease in the average perpendicular lattice constant for the epi-layer.

A 1000 Å thick and a 1 μm thick unbombarded (GaIn)As layers, the samples "1" and "2" in Table 1, were annealed isochronally for 15 minutes from 100 °C to 500 °C at approximately 100 °C steps (same as in Fig.5 (B)). The LO phonon frequencies measured after the 400 °C and the 500 °C annealing steps were about 1 cm^{-1} greater than in the as-grown sample. According to the LO phonon frequency versus composition data for this ternary alloy, given in ref. 5, the

above result again indicates the indium loss in the thermally annealed (GaIn)As film at temperatures lower than about 500 °C.

A 1400 Å thick sample, which is the same as the sample "b" in Table 1, but unbombarded, was annealed at 850 °C with no protective cap, under an arsenic overpressure for 20 minutes. The depth-averaged x-ray strain, measured after the annealing, was about 0.16 % for the parallel strain and 0.90 % for the perpendicular strain. A substantial change is noted from the as-grown sample data: 0.02 % for the parallel strain and 1.20% for the perpendicular strain. A shallow-angle incidence asymmetric 224 rocking curve was analyzed using a dynamical diffraction theory analysis program [9]. A best fit of a calculated curve (solid curve in Fig.4) to the experimental curve (scattered dotted curve) was obtained as shown in Fig.4, using the depth profiles of a parallel x-ray strain (dotted horizontal line) and the perpendicular x-ray strain (solid staircase curve) which are shown in the inset of Fig.4. The indium concentration profile in the film shall approximately follow the perpendicular x-ray strain profile, and it shows a thermally induced indium out-diffusion phenomenon, clearly. During a thermal annealing even below 500 °C, a suitable protection cap is imperative to prevent the indium out-diffusion.

4.2 Annealing of MeV ion-bombarded (GaIn)As films

A 1000 Å and a 1 μm thick layers, the samples "1" and "2" in Table 1, which had been bombarded with the 15 MeV Cl ions, were isochronally annealed. The x-ray strains were measured after each annealing step. It was found that the parallel x-ray strain was fixed, independent of temperature, at 0 % ± 0.01% for the 1000 Å layer and at 0.32 % ± 0.02 % for the 1 μm layer. In Fig.5 (A), we

show the perpendicular x-ray strain as a function of the annealing temeprature for samples bombarded to 1.25×10^{15} ions/cm^2. The perpendicular lattice constants monotonically decreases with temerature due to a combined effect of radiation damage recovery and indium out-diffusion. It is, however, believed that damage recovery is the main cause for the decrease of perpendicular lattice constant at temperatures below about 500 °C. The indium out-diffusion in the layers, bombarded and annealed, should have been caused by both the bombardment and the annealing. Note the singinificantly lower perpendicular strain in the annealed sample "1" than in the as-grown sample which is indicated by a horizontal dotted line in the figure. This sample went through a precipitous derease of perpendicular lattice strain during the bombardment (see Fig.2).

Shown in Fig.5 (B) are the LO phonon frequencies for the similar samples, but bombarded to 2.5×10^{15} ions/cm^2. At 300 - 400 °C, the phonon frequency for both samples exceeds the frequency in the as-grown films. The frequencies for the as-grown samples are shown by the two dotted horizontal lines in the figure. It is believed that the radiation damage in the (GaIn)As layer is completely recovered by annealing up to 500 °C, and the excess frequency over the as-grown sample is due to the decreased indium concentration.

5. Conclusion

For the MeV ion-bombarded or thermally-annealed (GaIn)As/GaAs, we have presented the data on the lattice constants of deformed unit cells and on the phonon frequency shifts. The depth profiles of the lattice constants are obtained and presented for a (GaIn)As layer annealed at 850 °C. For films with

an initial in-plane lattice mismatch greater than 0.02%, the in-plane mismatch varies significantly with the MeV ion bombardment. For films with an initial in-plane mismatch less than 0.01%, the in-plane mismatch does not vary under the MeV ion-bombardment or the thermal annealing up to 500 °C. For layers with greater in-plane mismatchs, the thermal annealing up to 500 °C does not induce changes in the in-plane mismatch. However, a 850 °C annealing induces a substantial increase in the in-plane mismatch. For films with an in-plane mismatch less than 0.01%, a precipitous decrease of the perpendicular lattice constant was observed at a demage-energy deposition of 10^{19} - 10^{20} keV/cm^3.

References

1. H.B. Dietrich, in: Advanced Application of Ion Implantation, SPIE Proc. 530, 30 (1985).
2. J.W. Mayer, L. Erickson, and J.A. Davies, **Ion Implantation in Semiconductors** (Academic Press, New York, 1970).
3. C.R. Wie, Nucl. Instr. Meth. B24/25, 562 (1987).
4. C.R. Wie, G. Burns, F.H. Dacol, G.D. Pettit, and J.M. Woodall, submitted to Appl. Phys. Lett., April (1988).
5. G. Burns, C.R. Wie, F.H. Dacol, G.D. Pettit, and J.M. Woodall, Appl. Phys. Lett. 51, 1919 (1987).
6. D.R. Myers, G.W. Arnold, C.R. Hills, L.R. Dawson, and B.L. Doyle, Appl. Phys. Lett. 51, 820 (1987).
7. C.R. Wie, T.A. Tombrello, and T. Vreeland, Jr., Phys. Rev. B 33, 4083 (1986).
8. G. Burns, F.H. Dacol, C.R. Wie, E. Burstein, and M. Cardona, Solid State Commun. 62, 449 (1987).
9. C.R. Wie, T.A. Tombrello, and T. Vreeland, Jr., J. Appl. Phys. 59, 3743 (1986).

Table 1 Characteristics of the as-grown (GaIn)As layers. The x-value, thickness (h), and in-plane mismatch of the $Ga_{1-x}In_xAs$ layers are given, along with the ion beams and their energies used to bombard the samples.

Sample	x	h (Å)	in-plane mismatch (%)	ion beam
1	0.07	1,000	< 0.01	15 MeV Cl
2	0.07	10,000	0.39	15 MeV Cl
3	0.15	10,000	0.66	15 MeV Cl
a	0.12	1,100	< 0.01	9 MeV P
b	0.11	1,400	0.02	9 MeV P
c	0.11	1,700	0.04	9 MeV P
d	0.11	2,000	0.08	9 MeV P
e	0.12	2,500	0.24	9 MeV P
g	0.1	1,500	< 0.01	2 MeV He
h	0.1	2,500	0.32	2 MeV He
i	0.1	10,000	0.45	Heat-treated

FIGURE CAPTION

Fig.1 The in-plane mismatch is given as a function of the bombarding ion dose for the layers with an initial in-plane mismatch greater than 0.01 %. The data points in an open circle are the pre-bombardment values. The data symbols correspond to the sample numbers in the first column of Table 1.

Fig.2 The perpendicular x-ray strain is given as a function of the damage-energy deposition for the samples with an in-plane mismatch less than 0.01 %. The data points in an open circle are the values before bombardment.

Fig.3 For the 1 μm thick, well-relaxed samples, given are (A): the perpendicular x-ray strain, and (B): the LO phonon frequency shift as a function of the bombarding ion dose. The dotted horizontal lines represent the pre-bombardment values. The solid curve in (A) and the data point "B" in (B) are data for bulk GaAs(001) crystals.

Fig.4 The 224 experimental (scattered dotted curve) and calculated (solid curve) rocking curves are given for a 1400 Å thick (GaIn)As film annealed at 850 °C. The calculated curve was obtained with assuming the strain depth profiles shown in the inset (perpendicular = solid staircase curve, parallel = dotted horizontal line).

Fig.5 The annealing behaviors are shown for the samples, "1" and "2".

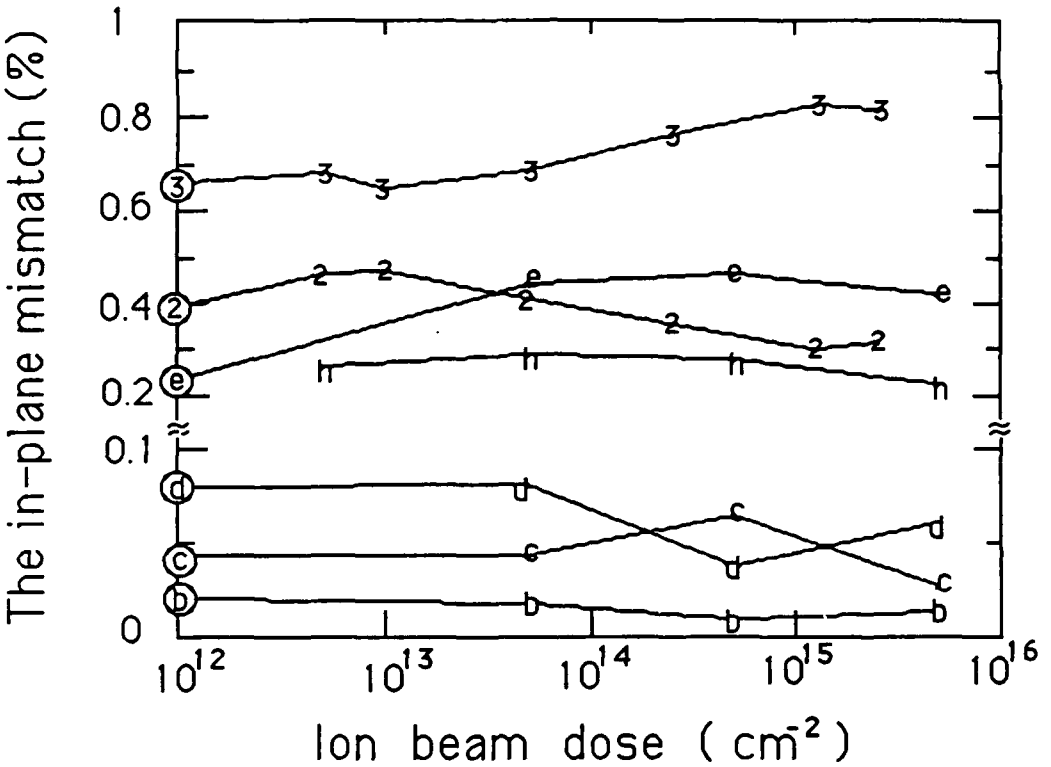
The in-plane mismatch (%)
1
0.8
0.6
0.4
0.2
0.1
0
10^{12}
10^{13}
10^{14}
10^{15}
10^{16}
Ion beam dose (cm^{-2})

Fig. 1

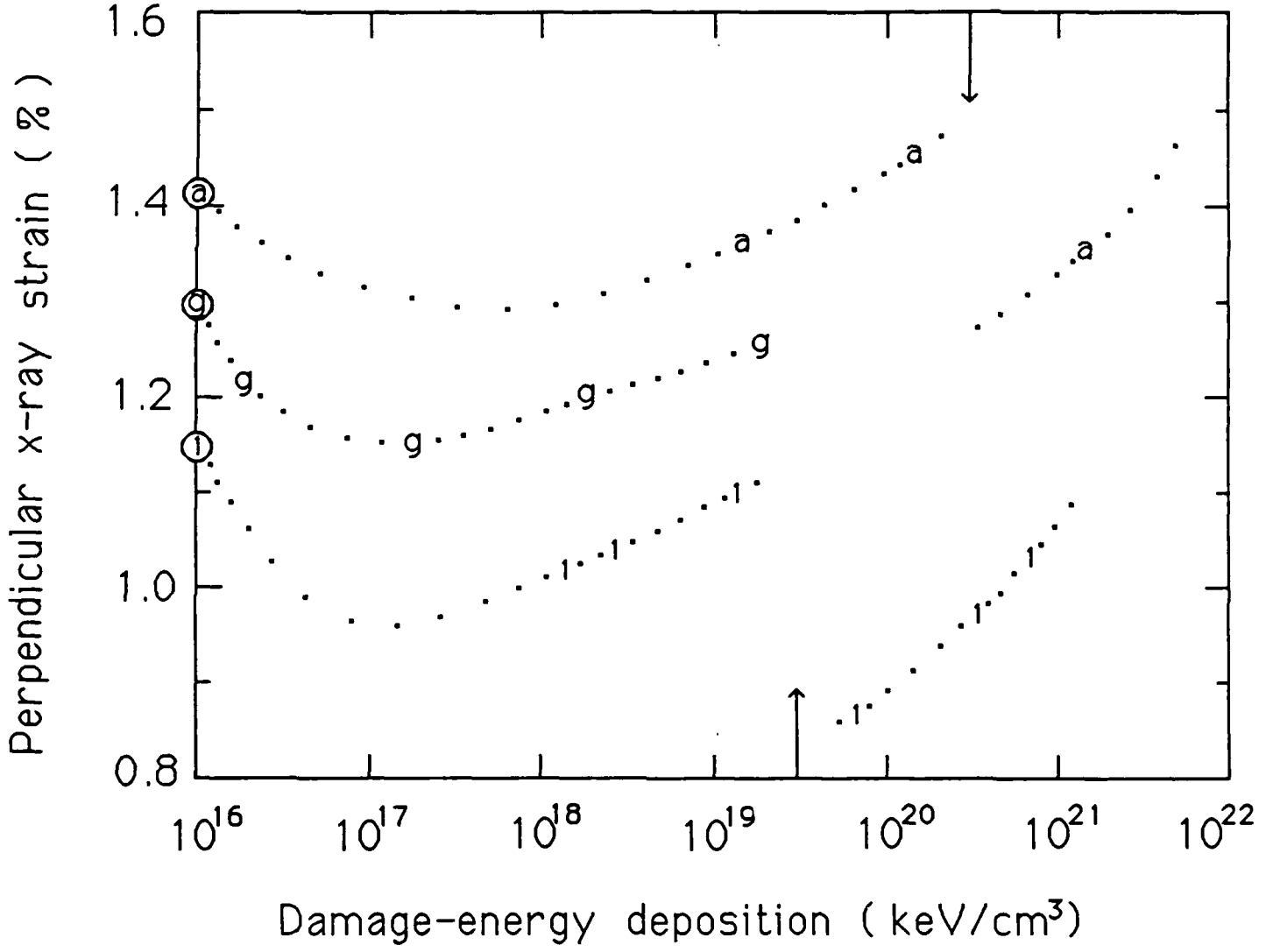
1.6
1.4
1.2
1.0
0.8
Perpendicular x-ray strain (%)
a
g
1
10^{16}
10^{17}
10^{18}
10^{19}
10^{20}
10^{21}
10^{22}
Damage-energy deposition (keV/cm^3)

Fig. 2

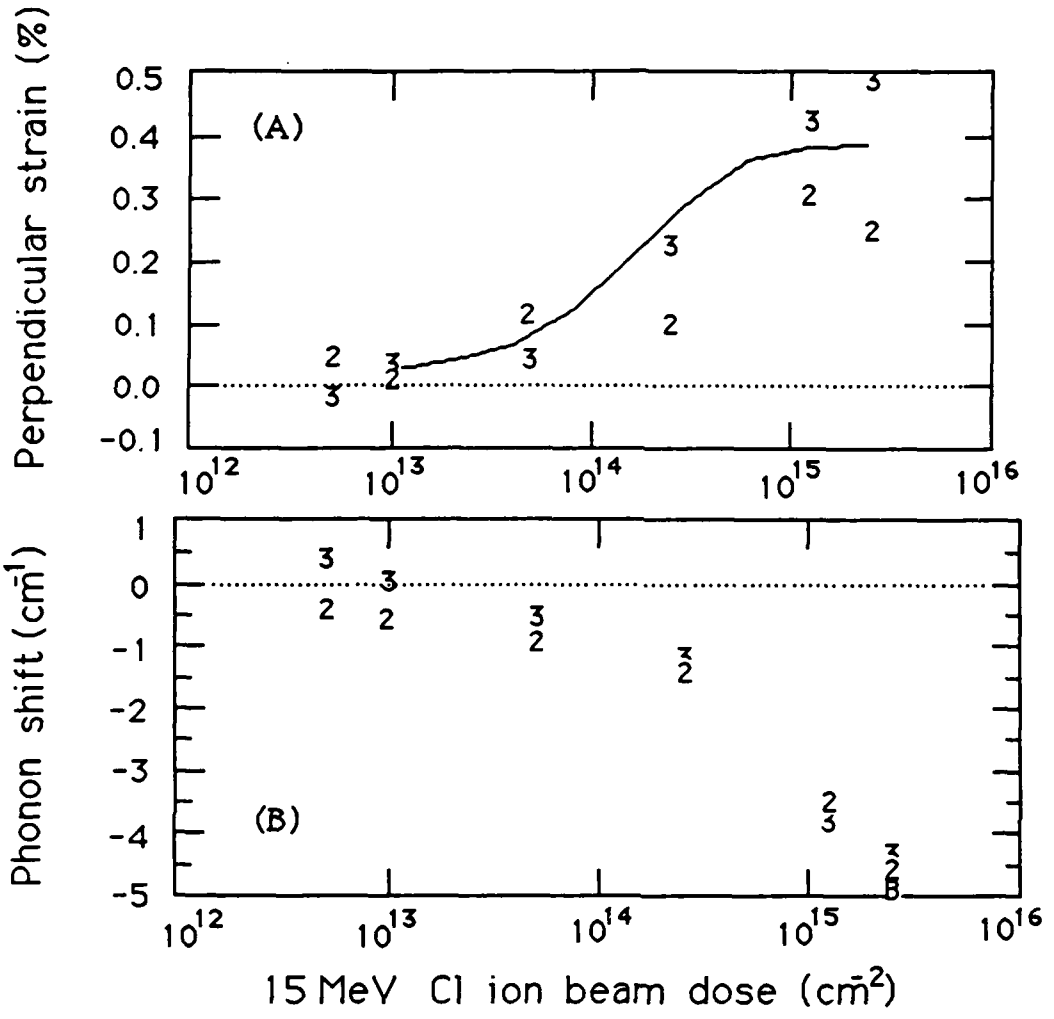
Perpendicular strain (%)
0.5
0.4
0.3
0.2
0.1
0.0
-0.1
(A)
10^{12}
10^{13}
10^{14}
10^{15}
10^{16}
Phonon shift (cm^{-1})
1
0
-1
-2
-3
-4
-5
(B)
15 MeV Cl ion beam dose (cm^{-2})

Fig. 3

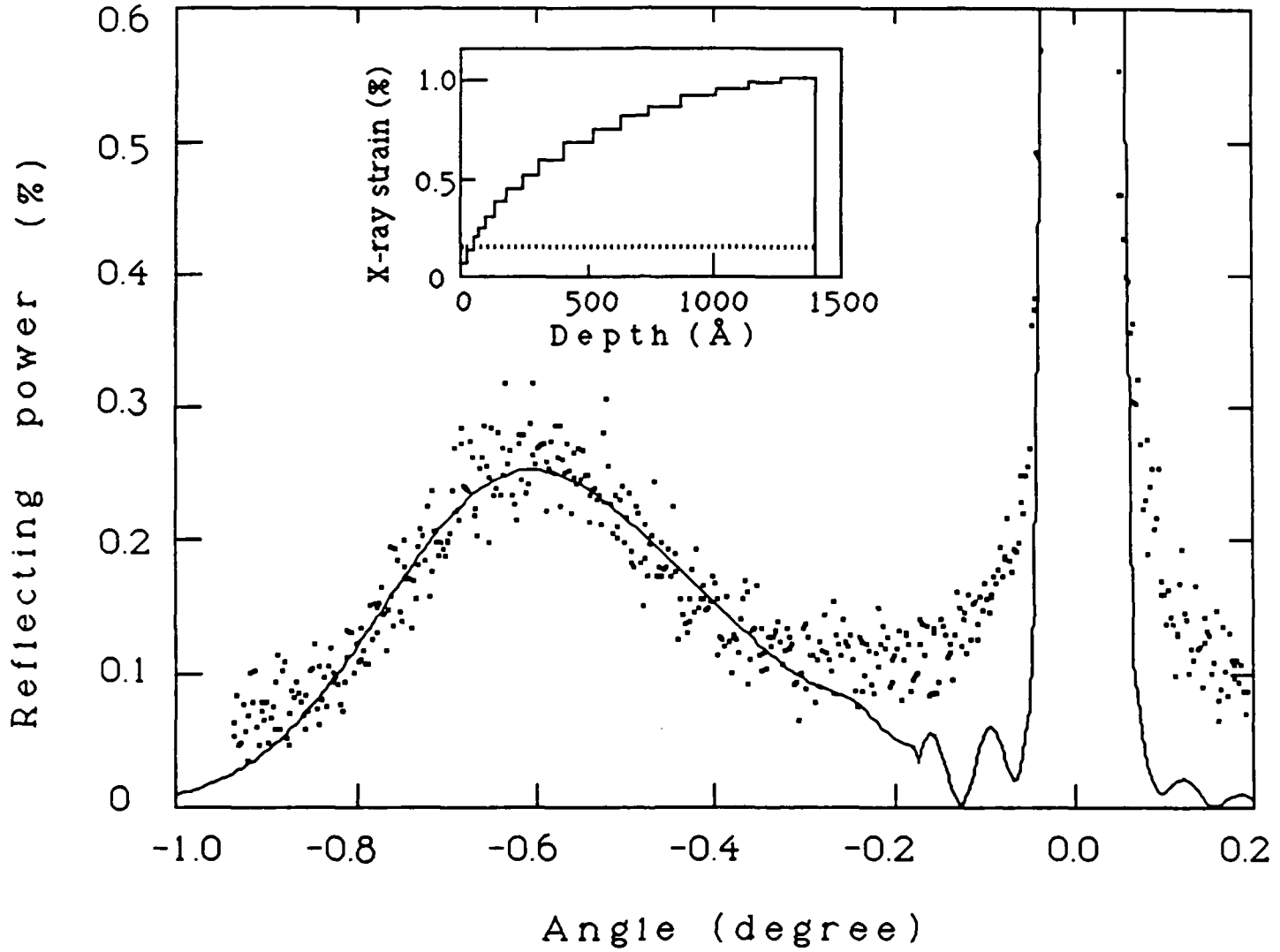
0.6
0.5
0.4
0.3
0.2
0.1
0
Reflecting power (%)
-1.0
-0.8
-0.6
-0.4
-0.2
0.0
0.2
Angle (degree)
X-ray strain (%)
1.0
0.5
0
0
500
1000
1500
Depth (Å)

Fig. 4

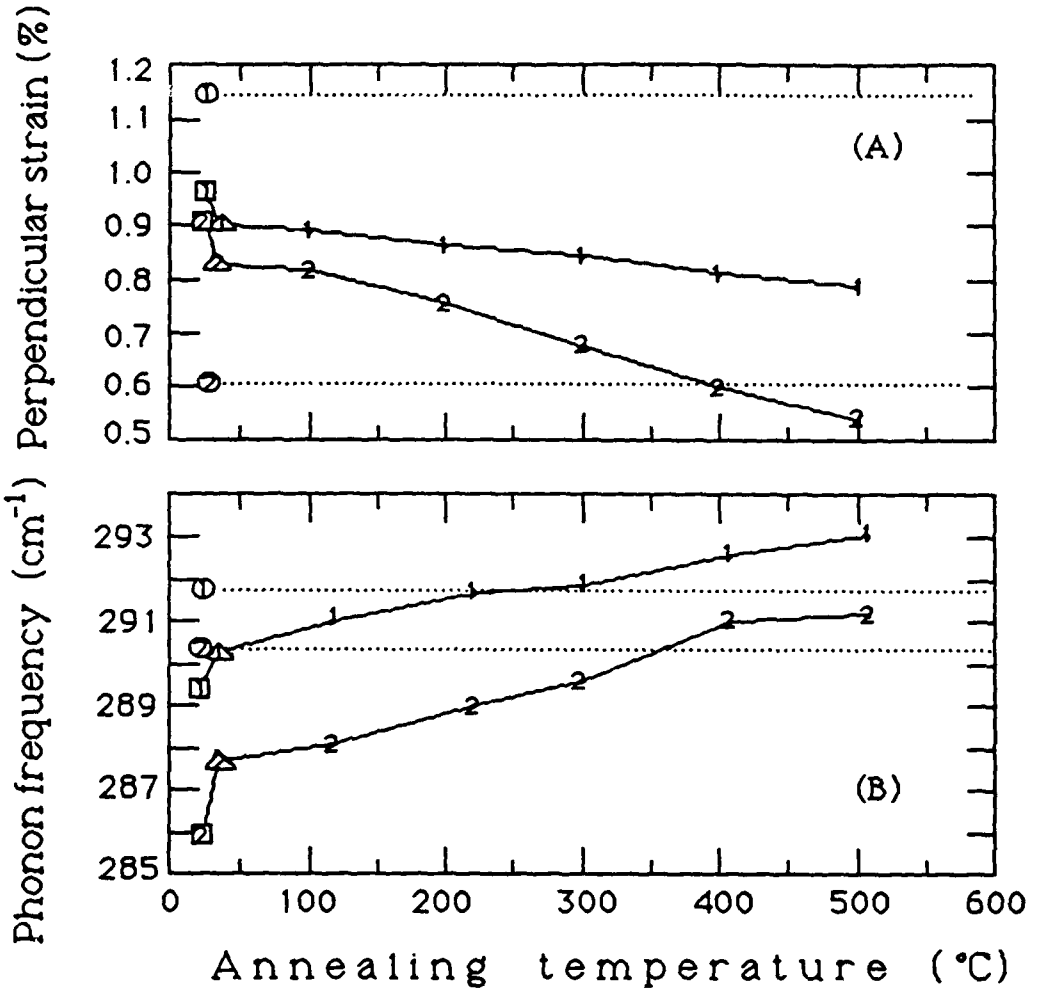
Phonon frequency (cm^{-1}) Perpendicular strain (%)
1.2
1.1
1.0
0.9
0.8
0.7
0.6
0.5
(A)
293
291
289
287
285
(B)
0
100
200
300
400
500
600
Annealing temperature (°C)

Fig. 5

MeV ION IMPLANTATION STUDIES ON LPE FILMS GROWN ON InP

T. T. BARDIN, J. G. PRONKO, and A. J. MARDINLY

Lockheed Research and Development Division, O/91-10, B203, 3251 Hanover St., Palo Alto, Ca, 94303-1191

C. R. WIE

Department of Electrical and Computer Engineering, SUNY at Buffalo, Amherst, NY 14260

ABSTRACT

Buried layers in devices fabricated from InP and epitaxially grown films on InP are often produced by MeV ion-implantation. This requires a need to better understand the effects of MeV ion beam damage. Samples of Fe-doped InP single crystal wafers (<100> orientation) with thin layers of LPE grown InGaAsP were prepared and implanted with 1.0 MeV $^{16}O^{+}$ ions at doses of $10^{15}/cm^{2}$. The as-implanted samples were analyzed by x-ray rocking curve technique to measure the radiation-induced lattice strain, the photo-luminescence spectroscopy for the study of shallow defect levels produced by MeV ions and the cross-sectional transmission electron microscopy (XTEM) to investigate crystalline changes due to the ion-implant. Changes in the near surface region where are compared to those near the end of the ion range.

Submitted to the 10th Conf. on the Application of Accelerators in Research and Industry, Nov. 1988. To be published in Nucl. Inst. and Meth. in Phys. Res. Vol B., (1989).

1. Introduction.

There has been a recent increase in the use of MeV ion-implantation to form buried deep-level insulator and semi-insulator layers in III-V materials [1]. These implanted layers serve to modify the electrical and optical properties of micro-electronic devices. Because of the high electron mobility in InP and the favorable emission wavelength of the InGaAsP/InP system, devices fabricated from ion-implanted InP and epitaxially grown films such as InGaAsP are playing a greater role in the VLSI industry as well as in opto-electronic fiber communication. However, in order to optimize the ion-implant process it is necessary to understand the influence of implantation on the material in terms of changes in structural and electrical properties.

The following is a description of the results of a study of the MeV-ion ($^{16}O^{+}$) implantation induced changes in electrical and structural properties of liquid phase epitaxially (LPE) grown InGaAsP films on InP substrates. The study focuses on the induced changes not only near the end of the ion range where ions deposit energy primarily by nuclear collisions but also near the implanted surface where high velocity ions interact mainly by electronic excitation with the encountered atoms. The existence of the thin quaternary layer on the surface tends to enhance the measurement of the near surface changes which would otherwise be difficult to observe if the sample were just an InP substrate. Ion-implantation induced changes in the electrical and structural properties were studied using x-ray rocking curve (XRC), cross-section TEM micrograph (XTEM), and photoluminescence (PL) measurements.

2. Experimental procedure and results

The sequential steps in the experimental procedure were: sample preparation, sample characterization, ion implantation, and characterization of ion-induced changes. The samples were implanted with 1-MeV $^{16}O^{+}$ ions at a dose of $10^{15}/cm^{2}$ using the Lockheed 3-MV Van de Graaff accelerator facility. This corresponded to an ion beam current of 36 nA over an area of 0.63 x 0.63 cm for 30 min. The face of the InGaAsP/InP samples were oriented to minimize channeling and the implantation was performed with the samples at room temperature.

2.1 Sample preparation and characterization

The samples were prepared by growing thin layers of InGaAsP on Fe-doped semi-insulating InP single crystal wafers (<100> orientation) by the liquid-phase epitaxy (LPE) process. The thickness of the films was measured by SEM micrography to be 0.85 $\pm$ 0.05 μm and was subsequently verified by x-ray rocking curve data which will be presented in the following section.

The film composition was determined from a combination of Rutherford backscattering (RBS) measurements and calculations using the energy band gap determined through photoluminescence measurements. The photoluminescence experiments were performed using He-Ne laser radiation of 632.8 nm to excite the near surface of samples held at a temperature of 12 K. The luminescence spectra were recorded using a McPherson 0.5-m scanning monochrometer with a 600 lines/mm grating and a cooled Ge detector. The photoluminescence emission spectrum from the surface of the sample before ion implantation is illustrated in Fig. 1. The sharp photopeak at 1050 nm represents emissions from the thin quaternary layer since 90% of the He-Ne laser light is absorbed within a depth of 0.5 μm [2],

well within the film thickness. This peak corresponds to an energy band gap of 1.181 eV. The energy band gap of the InP is known to be 1.4 eV (886 nm) and no contribution to the spectrum from the InP substrate is observed at this wavelength in the data of Fig. 1. By using the measured energy band gap value for the film in the calculation of Adachi [3] for the lowest direct electronic band gap in quaternary $In_{1-x}Ga_xAs_yP_{1-y}$ material, a composition of $In_{0.82}Ga_{0.18}As_{0.38}P_{0.62}$ with a relative error of ± 0.13 is obtained. The composition thus obtained is an average value for the film thickness weighted by the laser absorption cross-section. This composition was also consistent with Rutherford backscattering (RBS) measurements, allowing for the non-uniformity of the film composition and experimental uncertainties.

2.2 Ion implantation damage studies

Ion implantation induced changes can be studied by measuring strain, lattice displacement, structural changes, and point defects. Strain and lattice displacements in the quaternary film and substrate were measured by x-ray rocking curve techniques using Cu($K\alpha_1$) radiation. The strain depth profile was derived from fitting the x-ray rocking curve by dynamical x-ray diffraction theory [4] using the measured composition determined in the previous section as a parameter. The percentage strain measures the percentage difference between lattice constants of the film and substrate perpendicular to the InP substrate facial plane. Fig. 2a illustrates the strain depth profile for the 0.87-μm thick quaternary film before ion implantation. The structure factor for the film used in the x-ray simulation was In(0.89), Ga(0.11), As(0.23), and P(0.77). The small variation in strain of 0.12% from the film surface to the interface corresponds to a non-uniformity of the lattice spacing in the film. This phenomenon has been observed in the past with LPE grown quaternary films. The

cause of the lattice spacing variation can be thought of as due to a slight variation in composition, although in the fitting of the x-ray rocking curve the composition was assumed to be uniform. This means the strain profile is providing a first order correction to the composition parameter, since it is a more sensitive measurement. A negative strain means a smaller C-axis (perpendicular to the surface plane) in the film's unit cell.

The C-axis can be modified by the ion implantation and an example of this is shown in Fig. 2b. After ion beam implantation the strain in the film region was reduced by varying amounts over the film thickness. Two possible mechanisms can be responsible for this change. One possibility could be from expansion of the C-axis due to heating created by the electronic stopping of ions passing through this region. The electronic stopping transfers energy to lattice electrons which produce phonons and lattice heating. The other possibility could be due to beam-induced interdiffusion of constituent atoms in the film by the less probable nuclear collisions which take place in this region.

The root-mean-square lattice displacement caused by ion implantation was deduced from the dynamical x-ray diffraction theory [4]. The displacement in the film shown in Fig. 2b is approximately 0.2 ± 0.1 Å; this parameter is not sensitive enough to characterize the small degree of damage in the film.

Ion damage near the end of the 1.5 μm ion implantation range can be clearly observed in the InP substrate as shown by the data illustrated in Fig. 2b. This damage is due mainly to nuclear stopping caused by large momentum transfer between slow-moving ions and the substrate atoms. The negative strain is consistent with the lattice contraction phenomenon reported earlier in ion

damage studies in InP [5] and large lattice displacement is seen at the end of the beam range.

Structural damage caused by the ion beam implantation was studied by cross-sectional TEM. The specimen was prepared by mechanical polishing, dimple grinding and ion milling at liquid nitrogen temperatures using 3-keV argon ions in a Gatan dual ion mill. After ion milling the specimen was further etched by a 1-second dip in a 1% solution of bromine in methanol.

Fig. 3a illustrates an XTEM micrograph which shows an amorphized layer of approximately 450 nm thickness at a depth of about 1.5 μm. This depth corresponds to the end of the implanted beam range. The interface between the crystalline and amorphous material at the beam entrance side was sharper than the side on which the beam stopped. In the higher resolution TEM micrograph illustrated in Fig. 3b, both a high density of <111> stacking faults in the crystalline material and pockets of crystalline structure in the amorphous material are present near both interfaces.

There are a number of models [6,7] proposed to describe the fractions of mixed crystalline and amorphous structures observed in the XTEM data. Those models are all based on energy loss of the ion beam by nuclear collision near the end of the ion range. As the ion stops, nuclear collisions cause direct lattice displacements and generate heat which may reach the melting point of InP on an atomically local scale. The material melts but quenches quickly leaving a tiny amorphous region. The damaged regions, surrounded by rigid frameworks of undamaged lattice, cause lattice strains (as seen in Fig. 2b) and stacking faults. The heavily damaged crystalline layers at the amorphous-crystalline interfaces are predicted by ion beam straggling.

There is no visible structural damage near the surface in the high-resolution XTEM micrographs. This does not mean that there is no damage in the near-surface layers. The following reasons may be considered: The structural damage is in the form of isolated atomic displacements caused by ion collisions. The estimated fraction of atoms displaced is a few percent for a beam dosage of $10^{15}/cm^2$, assuming that the cross-section for atomic displacement due to nuclear collisions is typically $10^{-17}/cm^2$ for MeV ions [8]. XTEM is not sensitive to isolated point defects on an atomic scale. These defects, such as vacancies, interstitials, antisites, and impurity-generated traps, can be detected by low-temperature photoluminescence.

The photoluminescence emission was compared before and after ion implantation. Since the sensitive detection depth is less than 0.5 μm, data illustrated in Fig.1 is from the InGaAsP film only. The original 1050-nm peak shown in Fig. 1 disappears completely in data obtained from the sample after ion implantation. This suggests that high-energy ion beams produce a large number of defects which are effective centers for non-radiative recombination of photo-excited carriers. These centers can be surface states, bulk traps, or beam-injected impurity centers, all of which are expected to alter the electrical properties of the film.

3. Conclusions

Room-temperature MeV ion-beam implantation at doses of $10^{15}/cm^2$ creates heavy structural damage at the end of beam range. It creates a large number of surface states and/or recombination centers in the near-surface layer even though the nuclear stopping cross-section is small. Photoluminescence measurements together with x-ray rocking-curve and XTEM data forms a powerful

combination of techniques with which to study ion induced changes. Further work to correlate dose and annealing conditions with low-temperature luminescence bands, sheet resistivity, and carrier density is planned for the near future.

Acknowledgements

The authors would like to thank Dr. L. J. Dreis for help with the photoluminescence measurements and S. K. Ichiki for preparing the XTEM samples. This research was supported by the Lockheed Independent Research Fund at Lockheed and the ONR contract N00014-87-K-0799 at SUNY.

References

[1] H. B. Dietrich in Advanced Applications of Ion Implantation, SPIE Proc. 530 (1985) 30.

[2] Semiconductors and Semimetals, Vol. III, Optical Properties of III-V Compounds, R. K. Willardson and A. C. Beer, eds., Academic Press, p. 529 (1967).

[3] S. Adachi, J. Appl. Phys. 53 (1982), 8775

[4] C.R. Wie, T.A. Tombrello and T. Vreeland, Jr., J. Appl. Phys. 59 (1986) 3743.

[5] C.R. Wie, T. Jones, T.A. Tombrello, T. Vreeland, F. Xiong, Z. Zhou, G. Burns and F.H. Dacol, Mat. Res. Soc. Symp. Proc., 74 (1987) 517.

[6] D.K. Sadana, Nucl. Instr. and Meth. B7/8 (1985) 375.

[7] F. Xiong, C. W. Nieh, D. N. Jamieson, T. Vreeland, Jr., and T. A. Tombrello, Mat. Res. Soc. Symp. Proc. 100 (1988) 105.

[8] C.R. Wie, T.A. Tombrello, and T. Vreeland, Phys. Rev. B33 (1986) 4083.

FIGURE CAPTIONS

Fig. 1 Photoluminescence spectrum obtained from an as-grown sample of InGaAsP film on InP at T=12 K

Fig. 2a Depth distribution of a) perpendicular strain for an as-grown sample and b) strain and damage for the sample after ion implantation

Fig. 3 a) A low magnification XTEM micrograph of an $^{16}O^{+}$ ion-implanted sample, showing an amorphous layer with pockets of crystalline material present near the interfaces. The amorphized layer is approximately 450 nm thick at a depth of 1.5 μm. b) A high resolution TEM micrograph showing stacking faults in the crystalline material and microcrystallites in the amorphous material near the interface between the amorphous layer and crystalline substrate as a result of ion implantation.

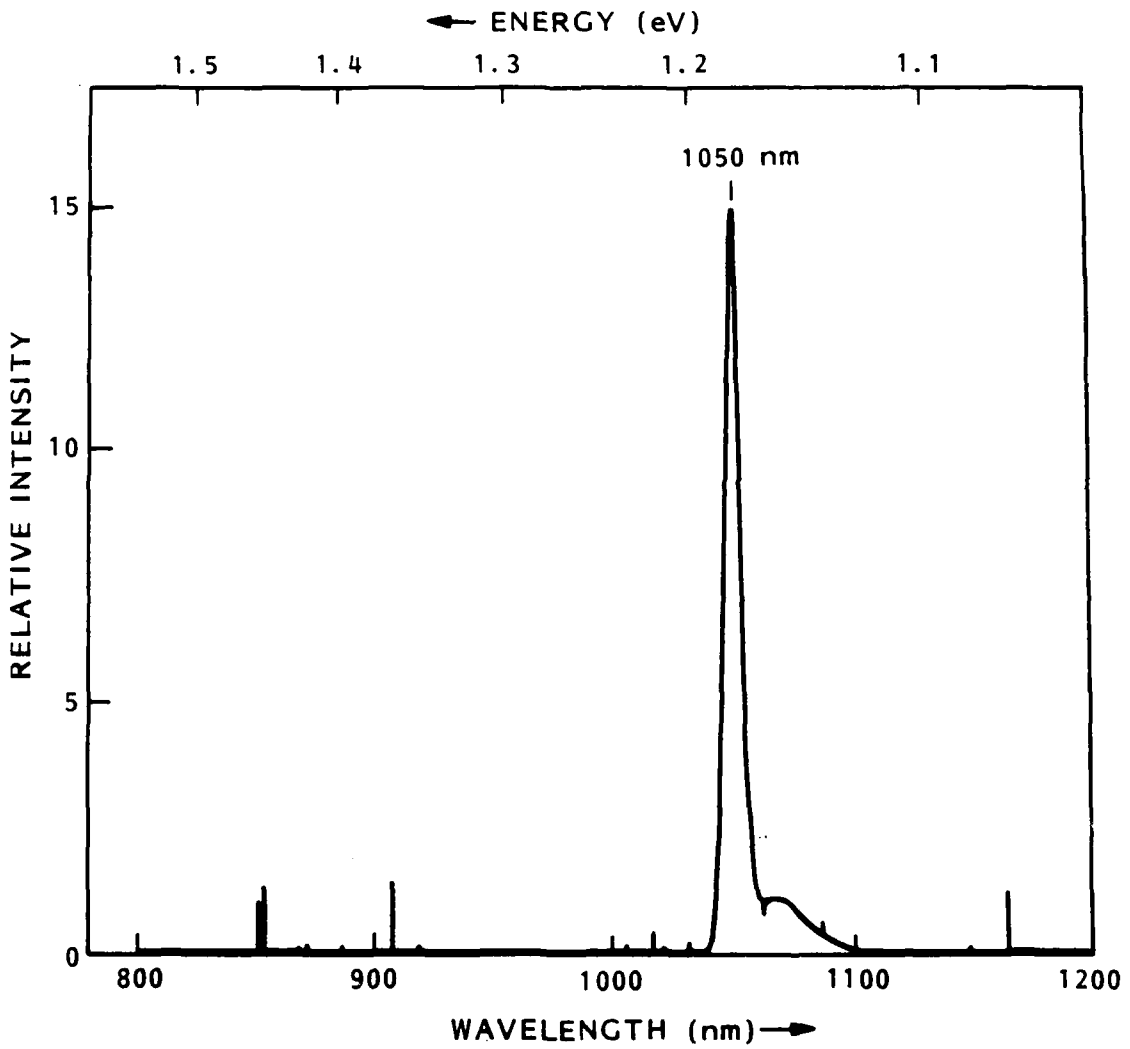
ENERGY (eV)
1.5
1.4
1.3
1.2
1.1
1050 nm
15
10
5
0
RELATIVE INTENSITY
800
900
1000
1100
1200
WAVELENGTH (nm)

Fig. 1

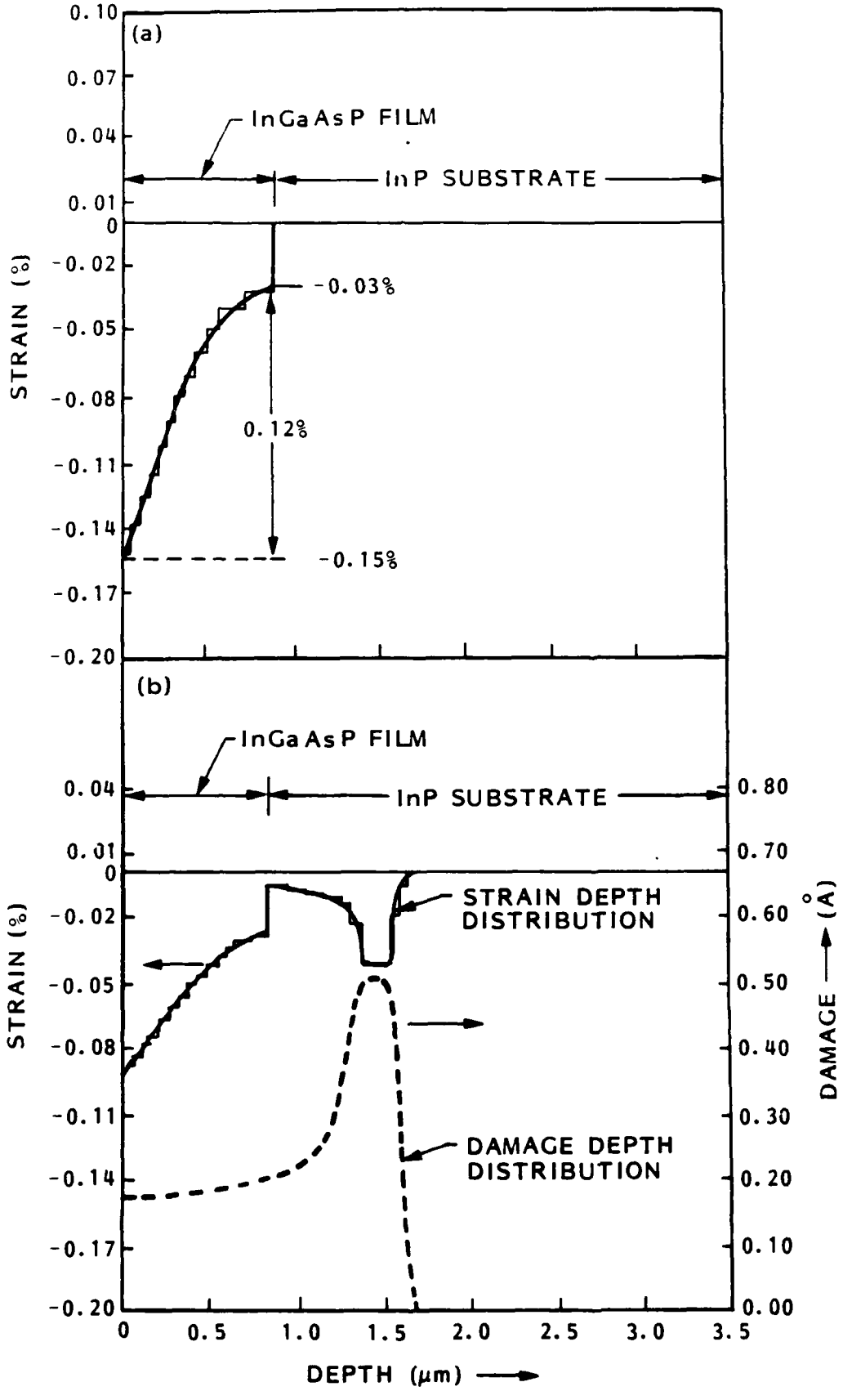
(a)
InGaAsP FILM
InP SUBSTRATE
-0.03%
0.12%
-0.15%
STRAIN (%)
(b)
InGaAsP FILM
InP SUBSTRATE
STRAIN DEPTH DISTRIBUTION
DAMAGE DEPTH DISTRIBUTION
DAMAGE (Å)
DEPTH (μm)

Fig. 2

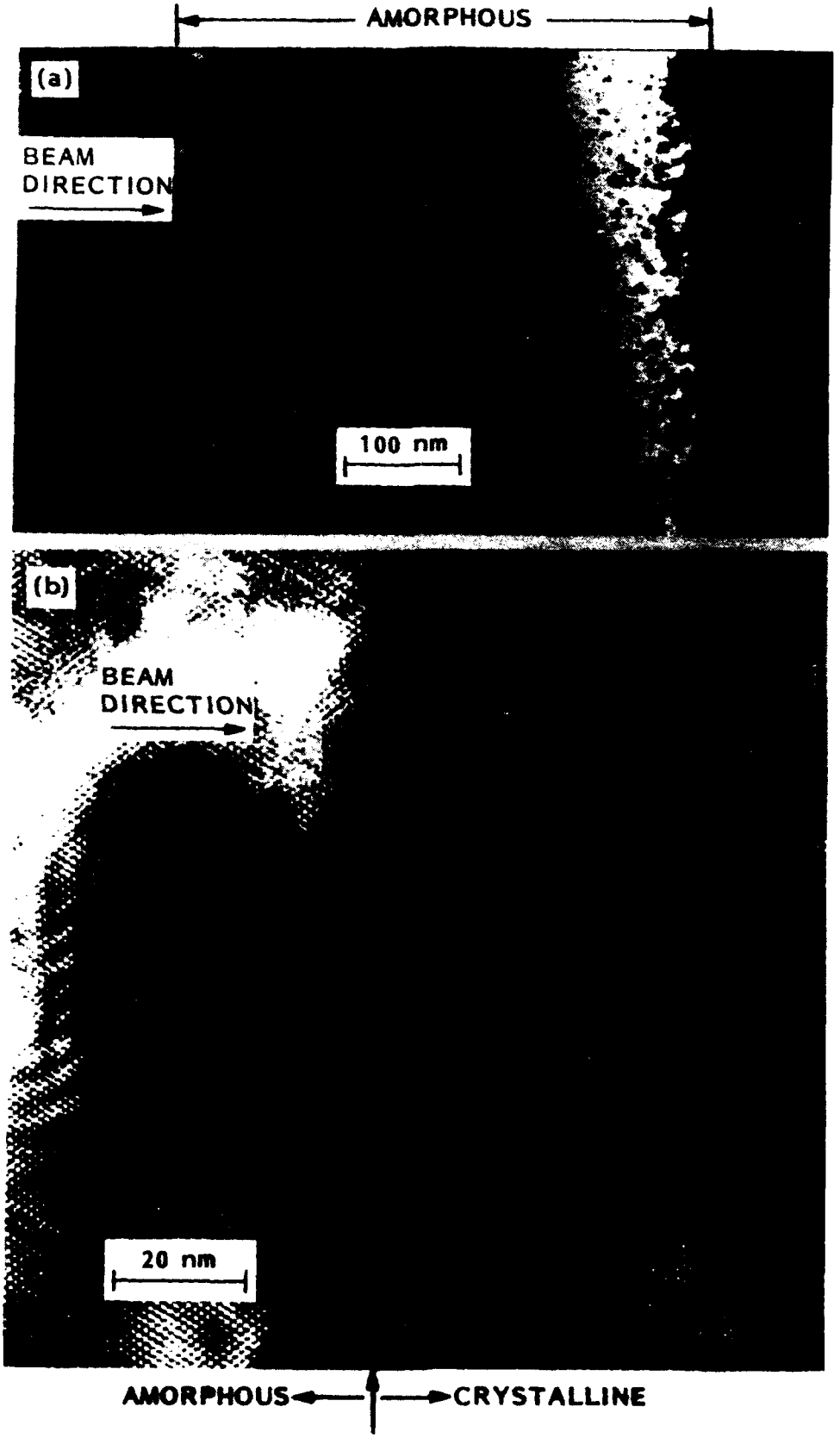
AMORPHOUS
(a)
BEAM
DIRECTION
100 nm
(b)
BEAM
DIRECTION
20 nm
AMORPHOUS
CRYSTALLINE

Fig. 3